Cancer Nanotechnology

RESEARCH Open Access

Evaluation of the anticancer potential of CD44 targeted vincristine nanoformulation in prostate cancer xenograft model: a multi-dynamic approach for advanced pharmacokinetic evaluation

Faiza Naseer[1,2*], Kousain Kousar[1], Maisa S. Abduh[3], Sadia Anjum[4] and Tahir Ahmad[1*]

*Correspondence:
faiza.naseer@ymail.com;
tahir@asab.nust.edu.pk

[1] Industrial Biotechnology, Atta-ur-Rahman School of Applied Biosciences, National University of Sciences and Technology, Islamabad, Pakistan
[2] Shifa College of Pharmaceutical Sciences, Shifa Tameer e Millat University, Islamabad, Pakistan
[3] Immune Responses in Different Diseases Research Group, Department of Medical Laboratory Sciences, Faculty of Applied Medical Sciences, King Abdul-Aziz University, Jeddah 21589, Saudi Arabia
[4] Department of Biology, University of Hail, Hail, Saudi Arabia

Abstract

The in vivo anticancer potential of vincristine (VC) loaded, thiolated chitosan-based nanoformulation (NFs) with an outer hyaluronic acid (VC-loaded in TCs-HA) coating was studied in prostate cancer (PC) xenograft in the immunosuppressed rat model induced by PC3 cell lines. Our previous study has already reported the in vitro efficacy of the said NFs. The ADMET Predictor (TM) Cloud version 10.4.0.5, 64-bit, was used to simulate VC's physicochemical and pharmacokinetic parameters. The percentage of encapsulation efficiency of VC by direct and indirect methods was 81.5 and 90%, respectively. Plasma samples from healthy rats showed improved pharmacokinetic and bioavailability profiles of NFs compared to VC injection via HPLC. The haemolytic analysis of NFs showed two times lesser toxicity to red blood cells. Xenograft rats showed maximum tumour volume up to 235 ± 0.02 mm^3 with increased body weight, and it was reduced by 56 ± 0.01 to 107.3 ± 0.03 mm^3 during the whole treatment by NFs compared to pure VC. The histopathology of the NFs group showed less malignancy with angiogenesis and significantly less metastasis to the liver and kidney. ELISA showed high expression of apoptotic biomarkers, including Bax, cleaved Caspase 3, and cleaved PARP, while the expression of BCL2, Caspase 3, COX-II, NFκB, and TNF-α was reduced. Immunohistochemical analysis also revealed that post-NF administration, cytoplasmic expressions of TNF-α and COX-II were reduced, as were nuclear expressions of NFκB. Thus, the prepared chemotherapeutic NFs were a comparatively potent oncolytic agent, safe with lesser off-target toxicity, and had an improved pharmacokinetic and bioavailability profile.

Keywords: ADMET predictor, Haemolytic analysis, HPLC analysis, Immunosuppression, Nanoformulation, Prostate cancer model, Pharmacokinetic parameters, Pk solver, PC3 cell line, Vincristine, Xenografts rat

Introduction

According to the International Agency for Research on Cancer (IARC) study, approximately ten hundred thousand new cases and six million cancer deaths are reported annually. Therefore, this disease is believed to become a global threat each year. There is a dire need to synthesize and introduce novel anticancer agents, drug delivery systems, and synergistic combinations of different chemotherapeutics as therapeutic modalities (Naseer et al. 2022a). The commonly available and widely used vincristine (VC), an M-phase cell cycle-specific antimitotic compound, inhibits the function of microtubules. These microtubules are polymeric fibres composed of α- and β-subunits of heterodimers. When large doses are administered, the VC acts by splitting the microtubule fibres and attaching the boundary of the β-subunit, resulting in spiralled fibre formation incapable of forming a mitotic spindle and separating chromatids during the mitosis (Škubník et al. 2020). This antimitotic activity is not limited to the spindle fibres of cancer cells; it also hampers the cell division of healthy cells. It disrupted the proliferation of progenitor cells in specific areas resulting in nausea, vomiting, diarrhoea, hair loss, myelosuppression, anaemia, and neutropenia.

The peripheral neuropathic symptoms, including numbness, tingling, and painful sensation in hands and feet, are also observed in patients using high doses/or long-term use of VC for cancer treatment (Verma et al. 2020). To reduce the VC dose, we previously reported surface functionalized NFs to efficiently and selectively deliver VC to the tumour site without significant systemic side effects, with promising in vitro results at normal and cancer cell pH. Several drug delivery systems, including macromolecular conjugation, polymersomes, polymeric micelles, and liposomes, have been studied for more safe and efficient delivery of chemotherapeutic drugs to tumour tissues (Taymouri et al. 2018). The encapsulation of VC into thiolated chitosan with HA coating NFs offers many advantages, such as improving mucoadhesion to the cell membrane, prolonging circulating time of the carrier, sustained drug release, reducing the off-target toxicity and increasing passive on-target efficacy (Naseer et al. 2022b) (Fig. 1).

The pharmacokinetic profile of commercially available VC is a very rapid initial distribution followed by a longer elimination half-life. The high tissue binding and diffuse distribution were observed due to its large volume of distribution. These features are tied to high drug exposure with limited delivery to the target area. The therapeutic purpose as a single effective regimen becomes compromised and leads to the use of multiple active entities (Silverman and Deitcher 2013). The reported data regarding VC-loaded TCs-HA NFs required extensive research on pharmacokinetic and bioavailability parameters after

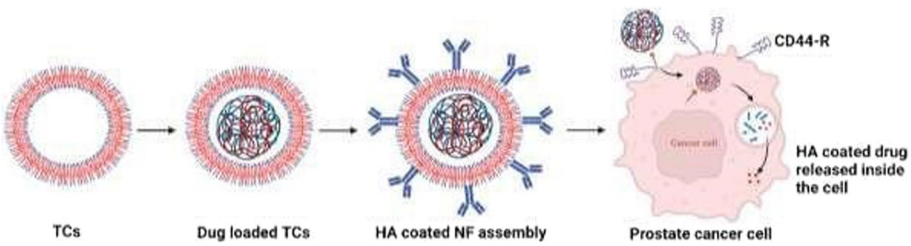

Fig. 1 Formulation of nanoformulation after encapsulation of VC into thiolated chitosan with HA coating for targeted delivering in prostate cancer cells at CD44 site

the administration of NFs in vivo. Therefore, tumour xenograft animals are mainly used in the in vivo study of drug delivery systems. They are used to introduce the effectiveness of therapeutic entities with anticancer potential by reducing tumour size, growth, and burden along with the various hallmarks of cancer, including tumour angiogenesis and metastasis (Jivrajani et al. 2014).

Researchers often employ immune-deficient nude or genetically modified animals to develop tumour xenografts. However, these animal models come with various limitations, including very high cost, Unavailability of hygienic conditions and sterile environment, high mortality rate, and lesser facilities for genetic modulation in developing countries. Some researchers reported that the nude animals might not precisely imitate the proper disease development due to excluding immune cells that play a crucial role in tumorigenesis (Firestone 2010). Different immunosuppression protocols include radiation, neonatal thymectomy, and immunosuppressive drugs (procarbazine, cyclophosphamide, etc.) to develop pharmacological immunosuppression in animal models. Many limitations are associated with these protocols, such as high expense, prolonged, frequent medication, making animals moribund, and models challenging to scale up. Therefore, the previously published method of developing a prostate cancer xenograft model using immunosuppressive drugs was applied (Aghasizadeh et al. 2022). Immunosuppressive drugs such as cyclosporine, an interleukin-1 and two-release inhibitor from macrophages, co-administered with an antifungal Ketoconazole, halt the proliferation and cause T-lymphocyte inactivation. Their coadministration increases cyclosporine's immunosuppressive effects and toxicity (Iyengar et al. 2013). Cyclophosphamide is a potent immunosuppressant and selectively suppresses antigen-specific cytotoxic T lymphocytes in a mouse model (Ahlmann and Hempel 2016).

Various cell lines, LNCaP, DU-145, and PC3 and their derivatives have been commonly used in prostate cancer-related research for decades, and these cells vary in androgen sensitivity, ability to grow, and metastatic ability. The PC3 cells lack androgen receptor (androgen insensitive) and prostate antigen-specific expression. They are the fastest-growing cell lines in vivo and were isolated from a bone marrow metastasis of a 62-year-old white male (McLean et al. 2017). Due to its metastasizing ability, the PC3 cell line is an excellent host for biomedical applications, including cancer therapeutics.

The current study successfully developed the prostate cancer xenograft rat model following the immunosuppression protocol using cyclosporine, ketoconazole, and cyclophosphamide administration. Then, the improved pharmacokinetic study of the novel VC-loaded NFs in TCsHA was explored through in vivo studies guided by predicted in silico assessments and is expected to be a benchmark in preclinical oncology research.

Materials and methods

Materials

Vincristine (purity > 98%), HPLC grade methanol, and acetonitrile were bought from J&K Scientific Ltd. (Shanghai, China). A Milli-Q purification system produced phosphate buffer saline, normal saline, and distilled water (Millipore, Billerica, MA, USA). Cell culture mediums, Roswell Park Memorial Institute medium (RPMI-1640), and Dulbecco's Modified Eagle Medium (DMEM) were bought from the Asian Scientific store in Islamabad, Pakistan. Fetal bovine serum (FBS), sodium bicarbonate, sodium pyruvate,

trypan blue, and trypsin were purchased from Gibco. The injections of cyclosporine, ketoconazole, cyclophosphamide, and amoxicillin were purchased from the Outpatient Department Pharmacy of Shifa International Hospital, Islamabad, Pakistan. The Rodent diet was prepared in the animal feed area of the animal house of Shifa Tameer e Millat University, Islamabad, Pakistan. Triton X-100, Matrigel, Disodium EDTA solution, injections of ketamine, cyclosporine, and xylocaine, and ketoconazole tablets were bought from the Outpatient Pharmacy of Shifa International Hospital Islamabad, Pakistan.

Molecular docking of VC with interactive proteins

The crystal structures of the potential VC target proteins were obtained from the Protein data bank (PDB.com), including Caspase-I (6BZ9), COX-II (1CX2), NFkB (1A3Q), and TNF-α (1CA4) for molecular docking studies. PyMOL 1.8 was used to evaluate the protein structure and cleaning of proteins manually, PyRx was used for the molecular docking study, and Discovery studio 2017 was used to visualize the docking results and interactions (Trott et al. 2010).

ADMET prediction of vincristine

The newest exploratory area in drug discovery is predictive ADMET studies. The goal is to develop computational models that connect structural alterations with changes in response using vast databases of ADMET data related to structures. From these models, compounds with superior attributes can be predicted and produced. These databases also allow users to extrapolate in vitro and in vivo ADMET values to predict human ADMET features (Davis and Riley 2004). They provide helpful information regarding existing molecules to help researchers develop these molecules into effective dosage forms. This study used the ADMET Predictor (TM) Cloud version 10.4.0.5, 64-bit edition, to predict several parameters, including metabolism, transporters, toxicity, and pharmacokinetic profiles for chemotherapeutic VC.

Prostate cancer cell line (PC3)

Prof. Dr Saeed Khan, Department of Molecular Pathology, Dow University of Health Sciences, Ojha Campus Karachi, Pakistan, generously provided the cells. These cells were seeded in 96 healthy plates with a seeding density of 1×10^4 in each well and placed in a humidified atmosphere of incubation at 37 °C with 95% air and 5% CO_2 to acquire the desired confluent layer of cells at their exponential growth phase (Jalilian et al. 2021). The media (RPMI-1640) was used to culture the cells along with the 1 mM sodium pyruvate, 2 mM l-glutamine, 4.5 g glucose/l, and 1.5 g/l sodium bicarbonate, and 500 µl of penicillin streptomycin (pen strep) with 10% FBS (Ghaferi et al., 2020).

Cell morphology analysis

Cell morphology analysis helps determine the physiological changes a cell undergoes after exposure to a specific treatment in a time and dose-dependent manner. Cell modifications such as rounding of cells, detachment, and shrinkage are hallmarks of cellular stress or apoptosis in response to treatment. It has been observed that anticancer agents produce cytopathic effects on cancer cells in a time and dose-dependent manner. For

this purpose, PC3 cells were cultured in a 96-well plate at 1×10^6 (100 µl) cell density and incubated for 24 h at 37 °C with 5% CO_2 (Naseer et al. 2021; Shao et al. 2018).

Cytotoxicity potential analysis

The cytotoxic effect of NFs of VC-loaded TCs-HA and pure VC was analysed following trypan blue exclusion assay, performed on prostate cancer (PC3) cells and human normal prostate epithelial cells (HPrEc). For this purpose, cells were plated in a 24-well plate at 130,000 cells/well density. The supernatant was removed after 24 h, and cells were detached and harvested using trypsin–EDTA (Gibco, New York) at 37 °C. A growth medium was added to stop the trypsin reaction, and centrifugation at 800 rpm for approximately 4 min was done to collect the cell palette. The PBS was used to wash the cells. The cells were resuspended in 1 ml of fresh media. 50 µl of 0.4% trypan blue (Gibco, USA) was mixed with 50 µl of suspended cells and incubated at 37 °C for 3 min. The mixture was then transferred to a hemacytometer for counting viable (white) and dead (blue) cells under a phase contrast inverted microscope. The counting of cells should begin within 5 min of mixing cells with dye (Kousar et al., 2023a, b). The percentage of cytotoxicity was calculated using the formula:

$$\text{Cytotoxicity \%} : \frac{\text{Absorbance of cells treated with NFs}}{\text{Absorbance of control cells}} \times 100.$$

HPLC analysis

To quantify the amount of VC loaded in the NFs and released in the plasma samples of rats was determined by high-performance liquid chromatography (HPLC). The system is composed of a Shimadzu series 200 chromatographic system (Shimadzu, Kyoto, Japan) with a binary pump and an SPD-20A UV–vis detector. The analysis was performed on a Dikma Dimonsil C18 column (150 mm × 4.6 mm, 5 µm, Dikma Technologies, China). The column was adjusted at the wavelength 269 nm for UV–vis detection at 25 ℃ with 20 µl injection volume. The mobile phase composition was a mixture of methanol and acetonitrile (60:40, *v*/*v*) with a 1 ml/min flow rate. The previously published formulas calculated the encapsulation efficiency (EE) percentages. Instrumentation and chromatographic conditions for in vivo quantification in plasma samples were adopted similarly to in vitro conditions (Silvestro et al. 2020; Naseer et al. 2022a, b, c, d).

Encapsulation efficiency (EE) percentage

Both direct and indirect methods were used to calculate the EE of NFs of VC-loaded TCs-HA. The centrifugation of the novel formulation was done for 1 h at 13,500 rpm to check the quantity of VC in the supernatant. The collected supernatant was filtered with a Millipore syringe filter size range of 0.45 µm, and the presence of free drug was analysed by HPLC (Jahan et al. 2021).

In vivo pharmacokinetics studies

An animal-based pharmacokinetic study was established to investigate whether there was an improved pharmacokinetic behaviour after administering NFs of VC-loaded TCs-HA compared to commercially available VC injection. Albino 8 to 10-week-old

male rats weighing approximately 200–250 g were taken from Atta-ur-Rahman School of Applied Biosciences (ASAB) animal house, National University of Science and Technology (NUST), Islamabad Pakistan, under the Ethical approval no. 04-2022-ASAB-01/02. The rats were housed at 22–25 °C with 60 ± 5% relative humidity. The balanced rodent food pellet and water ad libitum were provided to animals with the light: dark cycle for 12:12 h regularly (Yu et al. 2015).

In vivo drug release study of NFs

Ten rats were randomly distributed into two groups, i.e. Group 1: VC injection and Group 2: NFs of VC-loaded TCs-HA. All animals fasted overnight with free access to water before administering the chemotherapeutic drug. The rats in Group 1 were administered a 1 mg/kg dose of VC injection into the tail vein. The other group was injected with 1 mg/kg NFs of VC-loaded TCs-HA, formulated by suspending freeze-dried powders of the NFs in 2 ml standard saline solution at the same dose as the control animals. After the administration, 1–2 ml of blood was collected from the tail vein at the predefined time points of 0, 0.5, 1, 6 and 24 h and stored in heparinized tubes with 100 IU per ml of blood. For plasma separation, the collected samples were centrifuged at 2300 $\times g$ for 5 min, stored at – 80 ℃ and analysed by HPLC at 269 nm (Chen et al. 2011; Yu et al. 2015).

Pharmacokinetic and bioavailability profile

The VC concentration in separated plasma samples was determined using the previously reported HPLC method with the liquid chromatography solution software (Shimadzu, Kyoto, Japan). The computer program Kinetica 4.0 (Thermo Electron Corp., USA) analysed the plasma concentration time data. The absorption half-life (t1/2 ka), elimination half-life (t1/2k10), the volume of distribution/bioavailability (V/F), total body clearance/bioavailability (CL/F), peak plasma concentration (Cmax), time to reach peak plasma concentration (Tmax), the total area under the concentration–time curve from zero to infinity (AUC 0–inf), and mean residence time (MRT) were the parameters analysed by the PK solver for both the VC injection and VC-loaded TCs-HA NFs (Chen et al. 2011; Yu et al. 2015).

Biodistribution of the prepared nanoparticles

The NFs of VC-loaded TCs-HA and pure VC were inoculated intravenously into ten rats. They were killed after a predefined period of 12 and 24 h of drug administration. The kidney, liver, stomach, spleen, lungs, and heart were saved. The blood samples were collected from the orbital sinus, heparinized, and centrifuged to obtain the plasma as previously described. The separated plasma and extracted organs were decomposed with heat using nitric acid. The VC concentration in the solution was measured by inductively coupled plasma mass spectrometry (ICP-MS) (Yu et al. 2015).

Haemolytic activity

The previously published method determined the haemolytic activity of the NFs of VC-loaded TCsHA (Shahzadi et al. 2019). 3 ml of fresh blood samples were collected in heparinized tubes from various volunteers after their counselling and consent. The blood

was centrifuged for 5 min at 1000 ×*g*, plasma was discarded, and cells were washed three times with 5 ml of chilled (4 °C) sterile isotonic PBS at pH 7.4. The concentration of erythrocytes was maintaine atd 10^8 cells/ml for each assay. 1 ml of NFs of VC-loaded TCs-HA of varying concentrations 5, 50, 500, and 5000 µg/ml was mixed with 1 ml of 3% *v*/*v* erythrocyte suspension. The same concentrations were prepared for VC injection. The samples were incubated for 35 min at 37 °C and agitated after 10 min. Immediately after incubation, the samples were placed on ice for 5 min and then centrifuged for 5 min at 1000 ×*g*. A 100 µl supernatant was taken from each tube and diluted ten times with chilled (4 °C) PBS. Triton X-100 (0.1% *v*/*v*) was a positive control, and phosphate buffer saline (PBS) was taken as a negative control. The absorbance was measured at 576 nm using µQuant (Biotech, USA). The % RBC lysis for each sample was calculated by the following formula:

$$\text{Percentage hemolysis} = \frac{\text{Abs. of sample} - \text{Abs. of blank}}{\text{Abs. of positive control}} \times 100.$$

All readings were taken in triplicate, and mean values were calculated (Jeswani et al. 2021).

Protocol for animal studies

The rats were allowed to acclimatize for one week before beginning the experiments. The NUST Institutional Review Board reviewed the experimental protocol before the start of the investigation. The animals were divided into four equal groups of 10 rats each. The first group was the control group (Buffer only), and Groups 2–4 were xenograft models. 2nd group served as the disease (prostate cancer), chemotherapeutic drug pure VC injection was administered to 3rd group. The prepared NFs of VC-loaded TCs-HA were given to the 4th group.

Immunosuppression

The oral route administered 10 mg/kg of ketoconazole and a dose of 30 mg/kg of cyclosporine by the intraperitoneal route every day for 7 days. The rats were given 0.1 µg/ml amoxicillin with drinking water during the study. The WBC profiling was carried out to determine the total white blood cells (WBC), lymphocyte, and neutrophils count to confirm the immunosuppression at the start of protocol (D-0), after 12 h of that day (D-0.5) and after a week (D-7). The cyclophosphamide was injected subcutaneously into rats at 60 mg/kg doses on days 1 and 3 before injecting the tumour cells after the peak immunosuppression. The blood samples were collected in a heparinized 1.5-ml tube from all rats by tail vein after applying lidocaine gel at the start of the protocol, at 12 h of the first day, and after 7 days. The WBC profiling was checked in an automated haematology analyzer (VetScan HM-5; Abaxis Inc., Union City, CA, USA) (Jivrajani et al. 2014).

Tumour implantation

Semi-confluent PC3 cells were trypsinized using 0.25% trypsin to detach the cells. The cells were centrifuged at 200 × g for 7 min at 4 °C, resuspended, and washed in the medium-growth RPMI1640. After washing, cells were resuspended in the growth medium. The cells were counted using a Neubauer chamber, and viability was

determined by MTT assay. The viable cells were stored on ice and injected immediately for tumour implantation. The hairs were removed by waxing with the blade of each immunocompromised albino male rat one day before injection. Of 0.1 ml PC3 cells mixed with Matrigel subcutaneously onto the right and left flanks with the following schedule for four days' implantation: every other day for three doses, as follows: 1×10^5 cells/3 ml (3.33×10^4 per dose $\times$ 3); 1×10^6 cells/3 ml (3.33×10^5 per dose $\times$ 3); 1×10^7 cells/3 ml (3.33×10^6 per dose $\times$ 3) and 5×10^7 cells/3 ml (1.66×10^7 per dose $\times$ 3) (Jivrajani et al. 2014; McLean et al. 2017).

Investigations of the xenograft model

Physiological parameters

The growth of the tumour was monitored at the injection site with close monitoring of clinical signs along with the measurement of the body weight of each animal. The tumour volume was observed and measured once/week externally by a digital calliper, and the following formula was used to calculate it: (width^2 $\times$ length $\times$ 0.5). The greatest longitudinal diameter was the length, and the greatest transverse diameter was selected as the width.

Haematological parameters Various parameters of WBC, such as neutrophils, lymphocytes, monocytes, eosinophils, basophils count, and morphology, were analysed. Likewise, different biochemical parameters of RBC such as RBC count, haemoglobin, haematocrit, MCV, MCH, MCHC, haemolysis and RBC morphology, and platelet count with morphology were studied from the blood taken from treatment groups and disease groups. The kidney function test (blood urea nitrogen and serum creatinine) and liver function test (alkaline phosphates, alanine transaminase, and aspartate aminotransferase) were also checked.

Biochemical parameters The whole blood was centrifuged at 5000 rpm per min for 10 min, and the serum was separated from the plasma. This serum was used to determine the levels of antioxidant enzymes, including superoxide dismutase (SOD), reduced glutathione (GSH), catalase (CAT), and malondialdehyde (MDA) levels of cancerous, treatment groups and control animals. The SOD levels were determined by formazan dye of the nitro blue tetrazolium (NBT) and optical density was checked at 560 nm while the reduced GSH levels were calculated when the yellow colour of sulfhydryl groups and DTNB [50, 50 (dithiobis 2-nitrobenzoic acid)] was obtained, and absorbance was checked at 412 nm. The concentration of CAT was determined with H_2O_2 and MDA levels with butylated hydroxytoluene (BHT) with the absorbance check at 240 nm and 532 nm in the UV visible spectrophotometer by following previously published protocols (Amar et al. 2019).

Histopathological studies

At the end of the study, tissues from tumour sites and vital organs of xenograft rats were saved from the rats and maintained in 10% neutral buffered formalin. The tissue samples were cut into 5-μm sections and stained with hematoxylin and eosin. The slices were observed and photo documented by optical microscopy (IX 51; Olympus, Tokyo, Japan)

equipped with a digital camera (TL4) to confirm the presence of malignant cells and the therapeutic efficacy of prepared NFs and chemotherapeutic drug.

Immunohistochemical studies

The slides were processed by an enzymatic method for antigen retrieval after deparaffinization and washed with PBS consecutively 3 × for 5 min. The slides were immersed in 3% H_2O_2 to quench endogenous peroxidase activity, followed by washing with PBS. The 5% normal goat serum was applied as a blocking serum to the slides and incubated for 2 h. The slides were incubated overnight with primary antibodies COX-II, NFκB, and TNF-α. The following day, slides were washed with PBS and incubated with the secondary antibody for 90 min, followed by 60 min incubation with an ABC kit (Santa Cruz) in a humidified box for 60 min. Slides were washed with PBS and stained with DAB, followed by dehydration with 70, 80, 90, and 100% ethanol. After dehydration, slides were fixed with xylene, and coverslips were placed with mounting media. Images were obtained using a light microscope and saved in TIFF format for further quantification by ImageJ software.

ELISA analysis

The extracted tissue samples were immediately put on ice-cold PBS and mixed with protease inhibitors. Then the samples were kept at − 80 °C for further homogenization. The samples were placed on a shaker at 4 °C for 2 h and centrifuged for 20 min at 13,000 rpm at 4 °C. The aliquot of the supernatant was collected in pre-chilled tubes, which were already placed on ice. The ELISA was performed to detect the protein expressions in the systemic circulation of xenograft rats, including Bax, BCL-2, cleaved PARP, and cleaved Caspase 3 by using rat Calbiotech ELISA kit for Bax, BCL-2, cleaved PARP and cleaved caspase-3 separately for control, prostate cancer, and treatment groups. The expression of COX-II, NFκB, and TNF-α proteins was also checked using a specific antibody rat Calbiotech ELISA kit.

Statistical studies

All the data were documented as the mean ± SD. One-way ANOVA analysis followed by post hoc Bonferroni correction was applied to determine the significance of differences among groups. The probability values with $p \leq 0.05$ were considered to be significant.

Results

Molecular docking of VC with interactive proteins

The docking of VC with Caspase-I (6BZ9) has shown hydrogen bonds, pi-alkyl interactions, alkyl, and conventional and carbon–hydrogen bonds. The binding energy was − 7.21 kcal/mol, indicating a solid interaction, as shown in Fig. 2A, a and Table 1. COX-II (1CX2) crystal structure consists of two identical chains, A and B. Its docking with VC has shown many hydrogen bonds (green dotted lines). All the binding distances were in the acceptable range and showed several different types of interactions. Nevertheless, overall, the binding affinity was − 8.0 kcal/mol indicating a solid interaction. The ligand showed two unfavourable positive interactions at HIS A: 356 (5.60 A°) and LYS A: 97 (5.24 A°) (Fig. 2B, b and Table 1). The docking of VC with

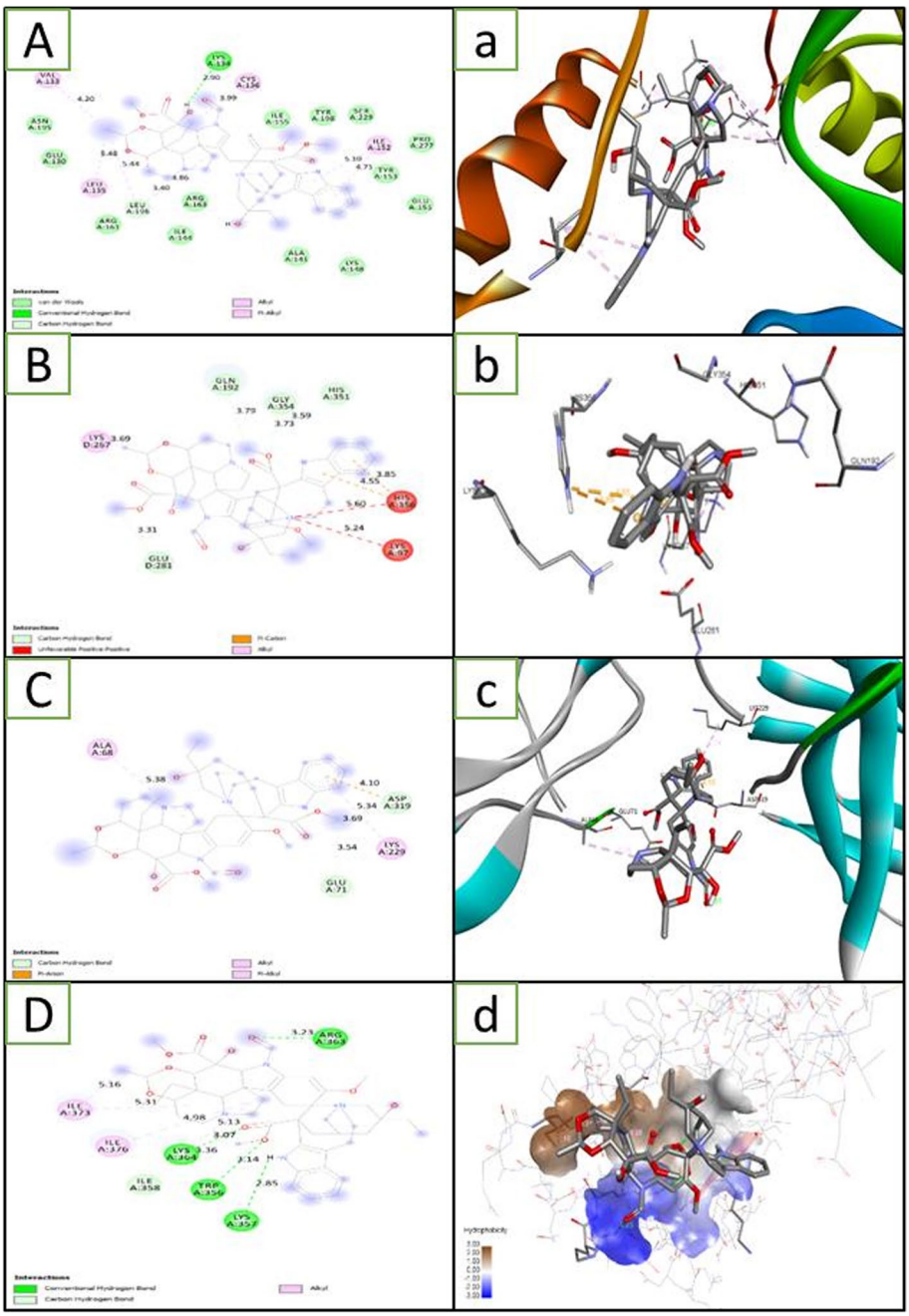

Fig. 2: 2D interactions and 3D interaction of VC with the amino acid residues of Caspase-I (6BZ9) [**A**, **a**], COX-II (1CX2) [**B**, **b**], NFκB (1A3Q) [**C**, **c**], and TNF-α (1CA4) [**D**, **d**], respectively. The green dotted lines show hydrogen bonds in the structures

NFκB (1A3Q) has shown fewer hydrogen bonds but more pi-alkyl interactions with − 8.1 kcal/mol binding energy. This protein showed more substantial interaction than the other proteins (Fig. 2C, c). The VC interaction with TNF-α (1CA4) has also shown more hydrogen bonds, pi-alkyl interactions, and fewer carbon–hydrogen bonds. The binding energy was − 7.0 kcal/mol (Fig. 2D, d).

Table 1 Binding energies, amino acid residues, binding distances and types of interaction among ligand and protein molecules

Name of protein (receptor)	PDB ID	Ligand	Binding energy ΔG	Amino acid residues	Distances A°	Type of interaction
Human Caspase-I	6BZ9	VC	− 7.2 kcal/mol	LYS A:134	2.90	Conventional H-Bond
				CYS A: 136	3.99	Pi-alkyl
				VAL A: 133	4.20	Pi-alkyl
				ILE A: 152	5.10	Pi-alkyl
				TYR A: 153	4.75	Vander Waal
				LEU A: 196	3.40	Vander Waal
				LEU A: 196	5.44	Pi-Alkyl
				LEU A: 135	5.48	Alkyl
				ARG A: 163	4.86	Vander Waal
Human COX-II	1CX2	VC	− 8.0 kcal/mol	GLN A: 192	3.79	C–H bond
				GLY A: 354	3.73	C–H bond
				HIS A: 351	3.59	C–H bond
				HIS A: 356	4.55, 3.85	Pi-Cation
				GLU A: 281	3.31	C–H bond
				HIS A: 356, LYS A: 97	5.60, 5.24	Unfavourable cationic-cationic
Human NFkB	1A3Q	VC	− 8.1 kcal/mol	ASP A: 319	4.10	Pi-anion
				ASP A: 319	5.34	C–H bond
				LYS A: 229	3.69	Pi-alkyl
				GLU A: 71	3.54	C–H bond
				ALA A: 68	5.38	Pi-alkyl
Human TNF-α	1CA4	VC	− 7.0 kcal/mol	ARG A: 363	3.23	H–bond
				LYS A: 364	3.07	H–bond
				LYS A: 364	5.13	Alkyl
				TRP A: 356	3.14	H–bond
				LYS A: 357	2.85	H–bond
				ILE A: 376	4.98	Alkyl
				ILE A: 373	5.31, 5.16	Alkyl
				ILE A: 358	3.36	C–H bond

ADMET prediction of vincristine

A) Predictive physicochemical values

Physicochemical properties are crucial for converting a molecular entity into an effective dosage form. The physicochemical characteristics of a molecule that are consistent with the possibility for good oral absorption are further refined by in-depth analyses exploring the relationship between metabolic stability and toxicity. Thorough examinations of the physicochemical components of drug–target interactions have strengthened these conclusions. Thermodynamic profiling reveals that the hallmark of best-in-class medications is a reliance on enthalpy, which is dependent on lipophilicity, to drive binding energetics (Meanwell 2011). The initial dose for VC used in this

Table 2 Predictive physicochemical profile of vincristine

Parameters	Predictive value	Explanation
MlogP	1.036009	Moriguchi estimation of log P. RMSE/MAE = 0.93/0.70
Permeation cornea	124.5494	Permeability through the rabbit cornea (cm/s × 10^{7}). RMSE/MAE = 0.40/0.32 log units
S + logP	3.300752	Simulations Plus model of log P. RMSE/MAE = 0.30/0.23
S + Acidic_pKa	11.39	Predicted macroscopic pKa that appear to be dominated by acidic functional groups. RMSE/MAE = 0.57/0.41
S + Basic pKa	7.69; 6.37	Predicted macroscopic pKa that appear to be dominated by basic functional groups. RMSE/MAE = 0.57/0.41
Solution factor	871.3152	Universal salt solubility factor based on S + Sw model
Vd	5.856062 L/Kg	Volume of distribution (L/kg) in human at steady state. RMSE/MAE = 0.40/0.30 log units (2D and 3D)
Diffusion coefficient	0.421147	Hayduk–Laudie infinite dilution diffusion coefficient (cm^2/s × 10^5) of nonelectrolytes in water
S + MDCK-LE permeability assay	Low	Apparent MDCK Transwell permeability (cm/s × 10^{7}). RMSE/MAE = 0.47/0.48 (2D and 3D) log units
S + logD	2.80345	Simulations Plus model of log P. RMSE/MAE = 0.30/0.23
BBB filter	Low (97%)	Predicts whether or not a compound can penetrate the blood brain barrier. Overall accuracy = 92%

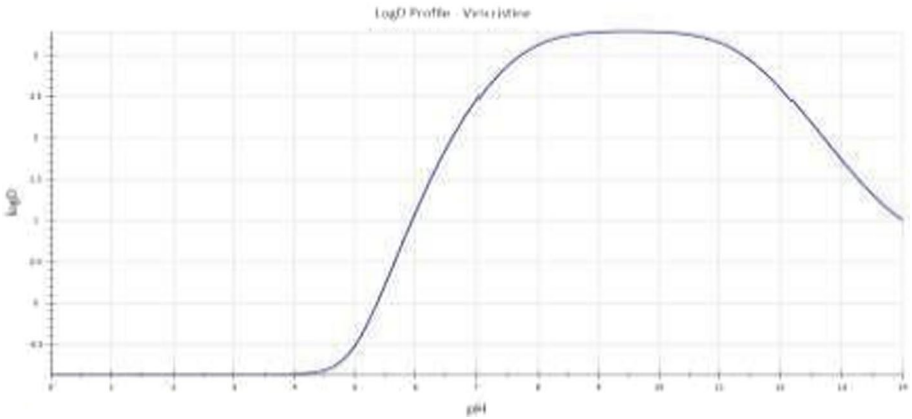

Fig. 3 Changes in LogD value with rising pH. Maximum 3.5 at 7.8 to 10.7 pH range

study was 1 mg/kg, and the predictive values were measured at 7.4 and 6.8 pH values. The predictive physicochemical profile of VC is shown in Table 2.

B) LogD (distribution coefficient)

LogD is a distribution coefficient widely used to measure the lipophilicity of ionizable compounds. The predictive logD values for VC depicted that the value of logD rises with the rise of pH and is maximum up to 3.5 in between the 7.8 to 10.7 pH range (Fig. 3).

C) pKa macrostates

The H^{+} concentration (pH) at which 50% of any drug exists in its ionized hydrophilic form in equilibrium with its un-ionized lipophilic form is known as the drug's pKa. The

greater the lipophilicity at physiological pH, the lower the pKa value. The value pKa represents a balanced aqueous solution's acidity and basicity. The molecules inside the drug must be electrically neutral to absorb; otherwise, it flows through the cell membrane. Figure 4 shows that at 11.39 pKa value, the drug was 99.9% available in a protonated form, and at 7.69 pKa, the drug was only 91.9% available but in an ionic form which ultimately affected the drug's ability to permeate the cellular membranes. On the other hand, the drug is 100% available at a 6.37 pKa value.

D) Predictive metabolic profile

According to the present data, it was predicted that VC acts as the inhibitor for CYP2D6 and CYP3A4, potentially affecting the metabolism of other drugs going concurrently with VC. Likewise, the Vmax value for the inhibition reaction with CYP3A4 was 31.138 Moles/min. On the other hand, the main metabolizing enzymes for VC were CYP3A4 liver microsomes and UGT1A3, which represent the substrate of VC to these enzymes.

E) Predictive transport profile

The transport proteins are essential for the distribution of drugs in the body. In silico tools, they have provided a complete set of data regarding the transport of VC based on the structure data, as shown in Table 3.

F) Predictive toxicity profile

The predictive data for vincristine showed that it is non-mutagenic but carcinogenic, hepatotoxic, and toxic to the reproductive system, along with no cardiovascular toxicity (Table 4). VC is an anticancer drug that acts on the polymerization phase of cell division and does not directly bind with genetic material, because of which the drug is non-mutagenic. Moreover, the drug has some chromosomal toxicity (60%), possibly due to several histone proteins on chromosomes. The predictive hERG inhibition value (4.626) represents that the drug is cardiotoxic, and the IC50 value was

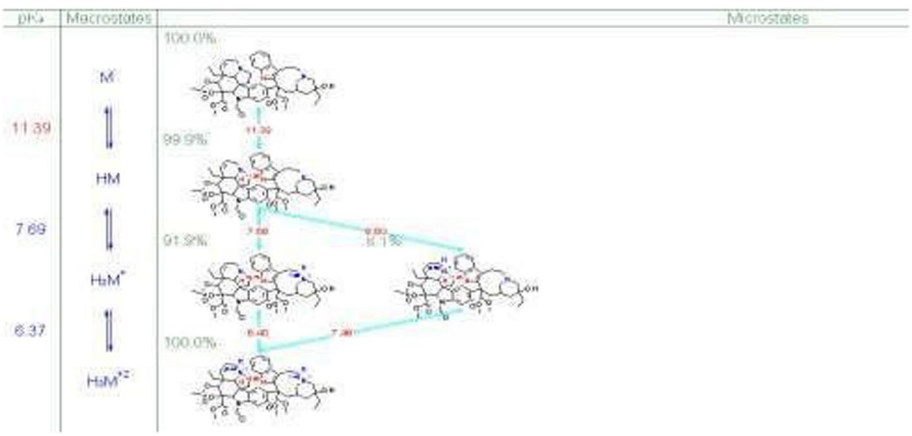

Fig. 4 Macrostates of VC and percentage of drug available at varying pKa values. The red-coloured values were for the macro-constants

Table 3 Vincristine interaction with transport proteins across the cellular membranes

Parameters	Predicted value	Explanation
P-glycoprotein (Pgp) substrate	Yes (99%)	Predicts whether or not the compound is P-glycoprotein substrate (Yes/No) Overall accuracy = 86%
P-glycoprotein (Pgp) inhibitor	Yes (97%)	Predicts whether or not the compound is P-glycoprotein inhibitor (Yes/No) Overall accuracy = 88%
OATP1B3 substrate	Yes (91%)	Predicts whether or not the compound is OATP1B3 substrate (Yes/No) Overall accuracy = 87.4%
OATP1B1 substrate	Yes (76%)	Predicts whether or not the compound is OATP1B1 substrate (Yes/No) Overall accuracy = 86%
OATP1B1 Km	2.911	Kinetic Michaelis–Menten atom-level Km constants in μM for OATP1B1 transporter. RMSE/MAE = 0.40/0.31 log units

Table 4 Vincristine predicted toxicity profile by interaction with different systems of the body

Parameters	Predicted values	Explanation
Mutagenic potential	Negative	
Chromosomal aberration	Toxic (60%)	Predicts whether or not the compound will trigger the mutagenic chromosomal aberrations Overall accuracy = 80%
hERG pIC50	4.62663374	Affinity to the hERG potassium channel in human expressed as pIC_50 in mol/L. RMSE/MAE = 0.55/0.43 in log units (2D and 3D)
P-Lipidosis	Negative	Qualitative estimation of causing phospholipidosis. Overall accuracy = 96%
Liver toxicity ALT	Yes Elevated 94%	Predicts whether or not the compound will cause elevation in the levels of SGPT enzyme Overall accuracy = 89%
AST	Elevated 46%	Predicts whether or not the compound will cause elevation in the levels of SGOT enzyme Overall accuracy = 84%
ALP	Elevated 48%	Predicts whether or not the compound will cause elevation in the levels of Alkaline Phosphatase enzyme. Overall accuracy = 91%
Serum GGT	Normal	Predicts whether or not the compound will cause elevation in the levels of GGT enzyme Overall accuracy = 94%
Serum LDH	Elevated 45%	Predicts whether or not the compound will cause elevation in the levels of LDH enzyme Overall accuracy = 95%
Reproductive toxicity	Yes (81%)	Qualitative estimation of reproductive/developmental toxicity. Overall accuracy = 90%
Rat TD50	0.271373	TD50 for rat carcinogenicity (mg/kg/day in oral dose) over a standard lifetime. RMSE/MAE = 0.54/0.42 (2D) and 0.52/0.43 (3D) in log units

considerable for toxic potential. VC was also found to interact with hepatic proteins, as was seen by its association with hepatic microsomes, which could lead to the drug's hepatic toxicity. VC's predictive liver toxicity profile has shown that it can potentially elevate several liver enzymes, such as AST, ALT, and ALP, which are the hallmark signs of liver damage. VC also possessed reproductive toxicity due to its action on normal and abnormal cell cycles. Moreover, several in silico tools are available today that can predict the early toxicity potential of drug molecules and the predicted

toxicity profiles of already existing drugs, which can later help researchers convert the existing drugs into effective dosage forms and delivery systems that minimize the toxic effects.

G) Predictive simulated pharmacokinetic profile

A plasma concentration (Cp) vs time curve was plotted using the cloud version of ADMET Predictor (TM) version 10.4.0.5, 64-bit. An initial 1 mg/kg dosage via IV route was used to predict the simulated pharmacokinetic parameters. Since the route of administration was intravenous, the bioavailability profile of the drug was nearly 100%. The Cmin and Cmax predictive values were 0.35 ng/ml and 4.12 ng/ml, respectively. Moreover, the area under the curve (AUC) was around 36.47 ng-h/ml, and the AUC inf was 39.92 ng-h/ml. The estimated half-life (t1/2) was 6.72 h from the Cp vs time curve, and 242.88 l was an apparent volume of distribution (Vd) which suggested that the drug can distribute over all parts of the body, specifically the fatty tissues, as shown in Fig. 5.

Cell morphology analysis

To investigate the cytopathic effect and drug efficacy of NFs of VC-loaded TCs-HA and pure VC PC3 cells were treated with different concentrations of 10, 50, and 90 µg/ml of 100 µl of NFs and pure drug for 24 h (concentrations were adjusted for dilution factor). The cell morphology was analysed using an inverted microscope at 12 and 24 h with a 10 × lens, as shown in Fig. 6. The results exhibited apoptosis of cells in a dose and time-dependent manner. The most negligible cytotoxicity was observed at 10 µg/ml. The concentration of 50 µg/ml showed a mild change in the shape of cells, while the highest toxicity was observed at 90 µg/ml, which was exhibited by rounding, detachment, and clumping of treated cells. The apoptosis induced in cells treated with NFs of VC-loaded TCs-HA was comparable to cells treated with a pure drug which

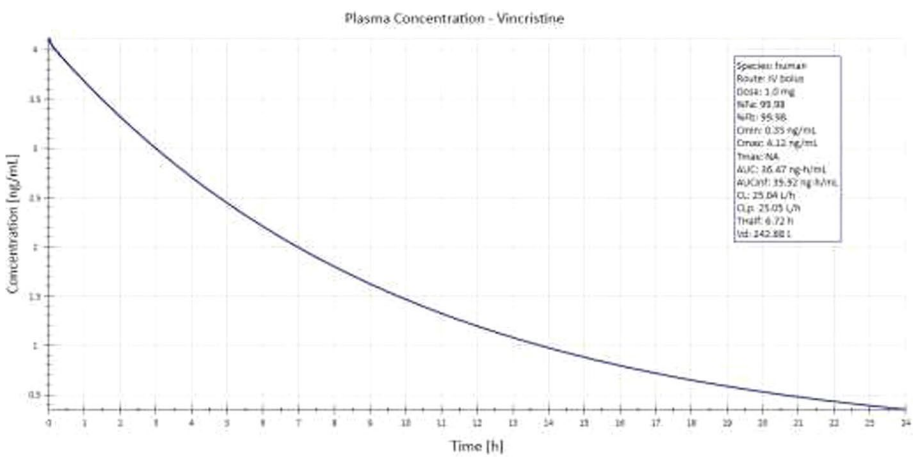

Fig. 5 Predictive simulated pharmacokinetic parameters for vincristine. Plasma concentration vs time curve for using 1 mg/kg as the initial IV dose (ADMET Predictor (TM) version 10.4.0.5, 64-bit)

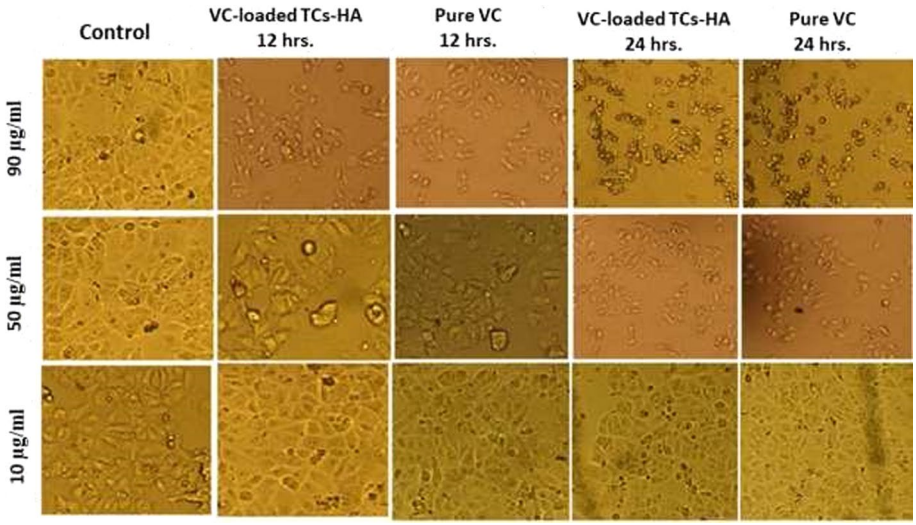

Fig. 6 Changes in cellular morphology of PC3 cells; dose and time-dependent response after treatment with nanoformulations of VC-loaded in TCs-HA as compared to pure vincristine

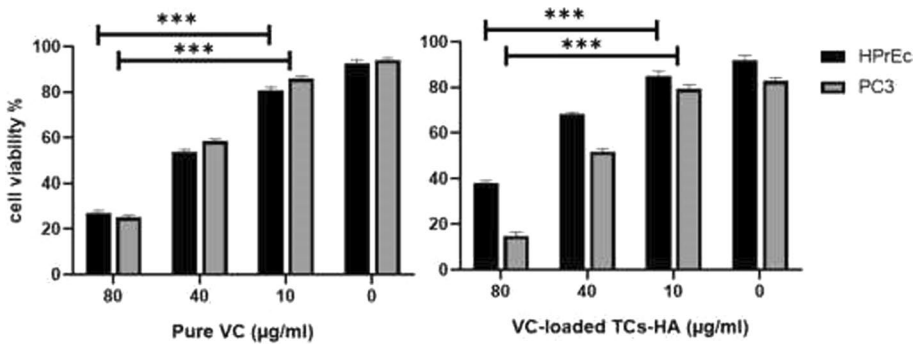

Fig. 7 Percentage of cell viability nanoformulations of VC-loaded in TCs-HA and pure VC-treated PC3 and HPrEc at a different concentration (mean ± SD, $p \leq 0.05$, *** highly significant)

confirmed that the prepared novel NFs could deliver the drug efficiently, maintaining its cytopathic effect while the targeted delivery capability of NFs spared the normal cells from this toxic effect of the drug.

Cytotoxicity potential analysis

For HPrEC treated with NFs of VC-loaded in TCs-HA blue exclusion assay showed that the maximum and minimum percentage cell viability was 85 ± 0.18% and 38 ± 0.02% at the concentration of 10 µg/ml and 80 µg/ml, respectively, compared to pure VC which showed 80.6 ± 0.04% and 26.8 ± 0.12% at the same concentration. The PC3 treated with NFs of VC-loaded in TCs-HA showed maximum cell viability of 79.2 ± 0.18% at 10 µg/ml and minimum 14.8 ± 0.02% at 80 µg/ml, respectively, and pure VC showed 85.8 ± 0.13% at 10 µg/ml and 25 ± 0.81% at 80 µg/ml as shown in Fig. 7. Hence, with an increase in the concentration of the drug in normal and cancerous cell lines, cell viability decreased.

Encapsulation efficiency (EE) percentage

To determine EE, a standard calibration curve of VC in distilled water was obtained by plotting a graph between different concentrations, including 0.2, 0.4, 0.6, 0.8, and 1.0 µg/ml of VC and their corresponding area under peak at 269 nm wavelength. The quantification of VC loaded into the NFs and released into the circulation from rat plasma samples was determined by HPLC. The average values of the percentage of EE of NFs of VC-loaded TCs-HA were 81.53 and 90.34% by the direct and indirect methods, as shown in Fig. 8, respectively.

Immunosuppression confirmed by WBC profiling

The concomitant administration of cyclosporine and ketoconazole at 30 mg/kg and 10 mg/kg, respectively, has induced significant immunosuppression in a dose-dependent manner compared to control groups. It was observed that no rat had shown any signs of toxicity or premature mortality due to Immunosuppression. The blood taken from healthy rats showed mean WBC, neutrophils, and lymphocyte counts of $7.51 + 0.01$, $4.36 + 0.02$, and $6.55 + 0.01 \times 10^3$ cells/µl, respectively, shown in Fig. 9a. These counts were reduced on the same day after 12 h of administration of drugs. On day 7, at the end of the protocol after administering cyclophosphamide injection, mean WBC, neutrophil, and lymphocyte counts were significantly reduced to 1.69 ± 0.01, 0.76 ± 0.01 and $1.46 \pm 0.02 \times 10^3$ cells/µl, respectively. Immunosuppression in rats was achieved at the end of the protocol after administering cyclophosphamide injection at a dose of 60 mg/kg on days 3 and 1 before tumour cell injection, as shown in Fig. 9b.

In vivo drug release study of NFs

The rats in Group 1 were injected in the tail vein with a dose of 1 mg/kg VC injection, and Group 2 with the same dose of NFs of VC-loaded TCs-HA. The plasma samples were collected at 0, 0.5, 1, 6, and 24 h to check the released drug concentration. The VC injection showed 9, 6.9, and 5.8 µg/ml release in the 0, half, and 1-h time interval and

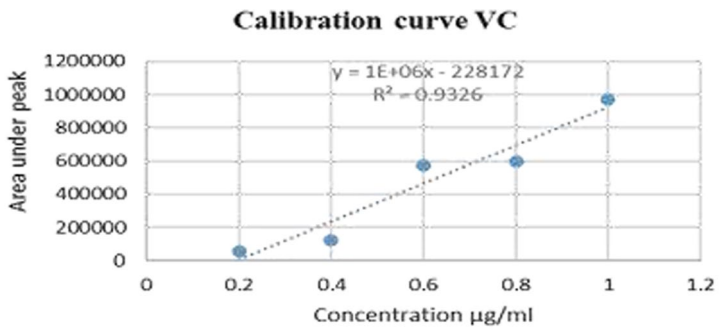

	Area under peak	EE%
Direct method	6036692.065	81.53457
Indirect method	884156.16	90.34901

Fig. 8 Encapsulation efficiency of nanoformulations of VC-loaded in TCs-HA by direct and indirect methods using the area under curve obtained by standard calibration curve of VC in distilled water

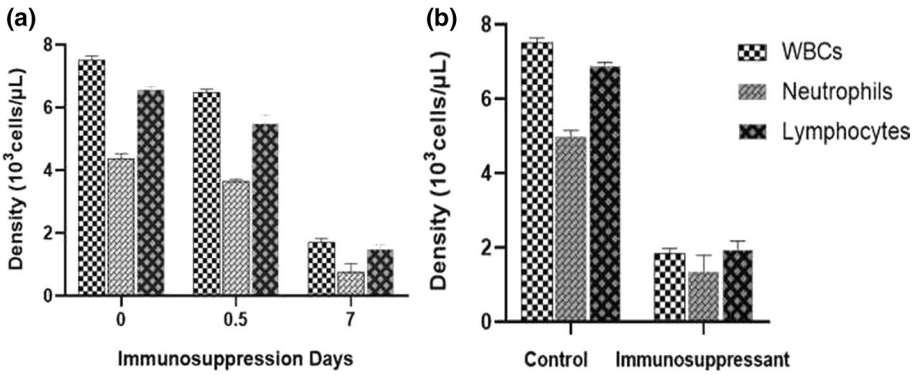

Fig. 9 Graph A shows the mean of WBC, neutrophil, and lymphocyte count at days 0, 0.5, and 7 in immunosuppressant animals, and graph B represents the whole protocol mean WBC, neutrophil and lymphocyte count of control and immunosuppressed rats after cyclophosphamide treatment ($n = 10$, mean ± SD, $p \leq 0.05$)

Marketed available VC inj.		
Time	Area under peak	Conc. (μg/ml)
0	10165550.35	9.02
0.5	7833294.89	6.99
1	6477093.99	5.82
6	785454.36	0.88
24	1158.85	0.19

NFs of VC loaded in TCs-HA		
Time	Area under peak	Conc. (μg/ml)
0	1960283	1.89
0.5	7045893.606	6.31
1	8402693.407	7.48
6	60474461.97	52.66
24	5992589.682	5.39

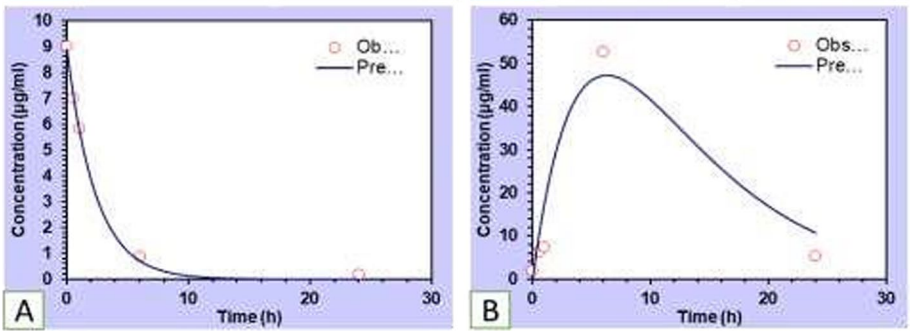

Fig. 10 Graphs plotted for different concentrations (μg/ml) for vincristine injection compared to NFs of VC-loaded TCs-HA. The prepared nanoformulations showed an improved area under peak at time points and provided sustained release of the drug for a longer time

showed that the plasma concentration was instantaneously achieved within minutes, but the NFs showed a 52% release of the drug in a very sustained manner up to 6 h, then the decline was observed in 24 h as shown in Fig. 10a and b.

Pharmacokinetic and bioavailability profile

The compartmental analysis showed a 1.6 h half-life for VC injection but 4.2 h for NFs. The total area under the concentration–time curve from zero to infinity (AUC 0–inf) was 21.07 μg/ml × h for injection (Fig. 11a) and 720–805 μg/ml × h for NFs. Thus, improved AUC provides sustained drug release from NFs prepared by the ionic gelation

Marketed available VC inj.

Parameter	Unit	Value
C0	µg/ml	8.872
k10	1/h	0.42

Parameter	Unit	Value
t1/2	h	1.6
V	(mg)/(µg/ml)	0.11
CL	(mg)/(µg/ml)/h	0.04
AUC 0-t	µg/ml*h	21.07
AUC 0-inf	µg/ml*h	21.07
AUMC	µg/ml*h^2	50.05
MRT	h	2.37
Vss	mg/(µg/ml)	0.11

A

NFs of VC loaded in TCs-HA

Parameter	Unit	Value
A intercept	µg/ml	3059.04
ka absorption rate	1/h	0.16
k10 elimination	1/h	0.16

Parameter	Unit	Value
t1/2ka	h	4.26
t1/2k10	h	4.44
V/F	(mg)/(µg/ml)	0.01
CL/F	(mg)/(µg/ml)/h	0.001
Tmax	h	6.28
Cmax	µg/ml	47.20
AUC 0-t	µg/ml*h	720.64
AUC 0-inf	µg/ml*h	805.72
AUMC	µg/ml*h^2	10119.95
MRT	h	12.56

B

Fig. 11 Compartmental analysis by Pk Solver showed the pharmacokinetic and bioavailability profile of nanoformulations of VC-loaded TCs-HA compared to the marketed injection of vincristine

method. The MRT was also improved from 2.375 to 12.56 h from injection to NFs. The CL and k10 were decreased from 0.04 to 0.001 mg/(µg/ml)/h and 0.4 to 0.1 1/h, respectively, for NFs, as shown in Fig. 11b. All parameters showed that NFs of NFs of VC-loaded TCs-HA stayed in the body for a more extended period and provided efficient pharmacological activity.

Biodistribution of the prepared NFs

After the intravenous injection of pure and NFs, the VC concentration was examined in the plasma, kidney, liver, spleen, lungs, heart, and brain. NFs showed a remarkably prolonged blood circulation time as compared to pure VC. The NFs maintained approximately 21% of the injected dose in the plasma after 24 h, but free VC was cleared rapidly from the blood circulation, maintaining approximately 1–2% of the injected dose at 24 h following intravenous injection. These results showed that prepared NFs of VC after coating with HA as a carrier may have an advantage over pure VC for improving blood circulation time. The prolonged circulation time also indicated a limited or delayed clearance of -NFs through the reticuloendothelial system.

The VC level reached its maximum concentration and was rapidly distributed in each organ within 5 min after the intravenous injection. Remarkably, the VC level in the kidney decreased from 14.93 ± 1.78 to 2.61 ± 0.21 µg/g from 5 min to 24 h, indicating a more significant amount of VC being excreted by glomerular filtration and a correspondingly high urinary VC concentration that leads to nephrotoxicity. However, NFs showed 7.39 ± 0.08 to 4.64 ± 1.18 µg/g from 5 min to 24 h with lesser nephrotoxic effects in rats (Yu et al. 2015). In contrast, the VC level in the significant clearance organs like the liver and spleen of rats treated with NFs was not significantly different from the first 5 min of injection to 24 h circulation showing prolonged blood circulation time, but there was a high difference with pure VC which leads to hepatotoxicity. The VC

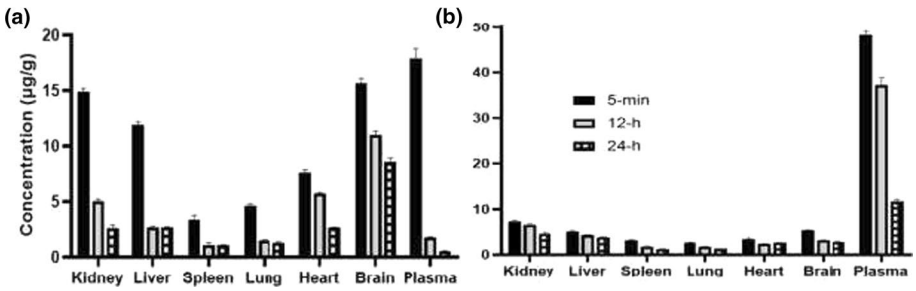

Fig. 12 Biodistribution of vincristine after a single intravenous injection (**A**) and nanoformulations of VC-loaded in TCs-HA (**B**) in rats. Each drug was administered to immunosuppressed rats at a dose of 1 mg/kg, and the data were presented where $n = 10$, mean ± SD, $p \leq 0.05$

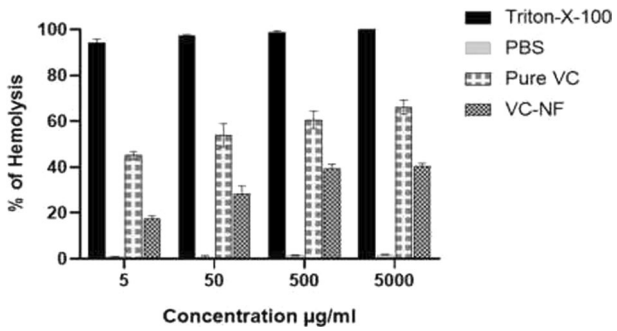

Fig. 13 Haemolysis by nanoformulations of VC-loaded in TCs-HA and pure VC as compared to positive 623 (Triton-X-100) and negative control (PBS) in pure blood taken from healthy volunteers, $n = 3$, mean ± SD, $p \leq 0.05$

concentration in the lung and heart gradually decreased after the intravenous injection of NFs from 2.66 ± 1.08 to 1.3 ± 0.02 µg/g and 3.5 ± 1.10 to 2.6 ± 0.01 µg/g from 5 min to 24 h, which was significantly lesser than pure VC. Consequently, pulmonary and cardiovascular toxicity was decreased in the NFs group of rats. The significant toxicity after 5 min of administration of pure VC showed 15.68 ± 1.21 µg/g in the brain and reduced to 8.55 ± 1.11 after 24 h, but in contrast, NFs exposed the rats to lesser neurotoxicity with a 5.3 ± 1.06 to 2.83 ± 0.09 µg/g in 24 h of intravenous administration as shown in Fig. 12.

Haemolytic activity

The NFs of VC-loaded TCs-HA showed 17.43 to 40.1% haemolysis in RBCs at 5 to 5000 µg/ml compared to pure VC, which showed 45.29 to 66% toxicity at the same concentration in pure blood taken from healthy volunteers as presented in Fig. 13.

Tumour implantation

The approximately 5×10^6 PC3 cells mixed with Matrigel on the flanks of immunocompromised rats were injected subcutaneously in groups 2 to 4. The palpable tumour was observed after a week from tumour cells injection and allowed to grow to 200 mm^3 for this study.

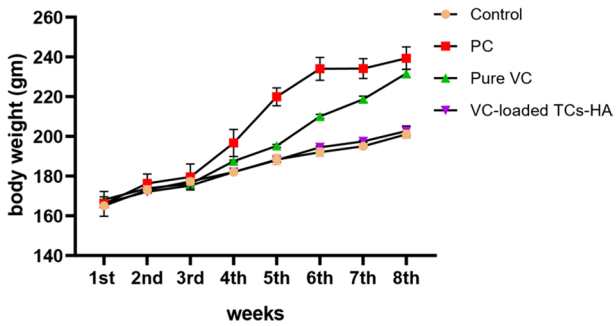

Fig. 14 Mean body weight each week after tumour implantation of PC3 cells in disease and treatment (pure VC and VC-NFs) groups; $n = 10$, mean ± SD, $p \leq 0.05$

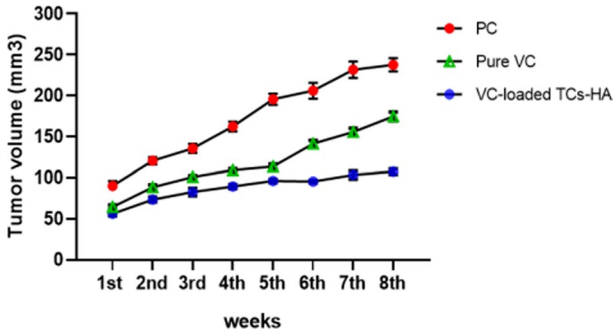

Fig. 15 Mean tumour volume (B) each week after tumour implantation of PC3 cells in disease and treatment (pure VC and VC-NFs) groups; $n = 10$, mean ± SD, $p \leq 0.05$

Physiological parameters

The mean body weight change and mean tumour volume was recorded each week after tumour implantation in the control, cancer, and treatment groups. The difference in mean body weight was significantly increased in the PC group compared to control animals, but the administration of NF showed a lesser weight increase than the administration of pure VC. The mean body weight of rats at the start of the experiment in control group 1 was 165 + 0.05 and increased to 201 + 0.03 g at the end. When the body weight of PC group 2 was recorded, it was 168.3 + 0.02 to 242.3 + 0.01 g from the first to the 8^{th} week. In the case of pure VC group 3, 168.1 + 0.07 to 231.6 + 0.09 g body weight was recorded, significantly more significant than the NFs of VC-loaded TCs-HA group 4, 57 + 0.03 to 204 + 0.05 g (Fig. 14).

It was also observed that the mean tumour volume radically increased from 93 + 0.01 to 235 + 0.02 mm^3 every week until the 8th week, and the growth of PC3 xenografts was found to be very aggressive. Group 3 was administered pure VC after three days of implantation of PC3 cells at the dose of 1 mg/kg once a week for 8 weeks, and tumour volume extended from 64 + 0.01 to 113.6 + 0.02 mm^3 till the 5th week after that, there was a sudden rise in tumour volume up to 174.6 mm^3 in 8th week. Group 4 received NF of VC-loaded TCs-HA, and it was observed that tumour volume was significantly smaller (56 + 0.01 to 107.3 + 0.02 mm^3) throughout the treatment as compared to pure VC (Fig. 15).

Haematological parameters

The RBC, WBC, and platelet profiles were checked in the blood of the treatment and diseased rat group. The NFs of the VC-loaded TCs-HA group showed improved RBC count $5.11 \pm 0.31 \times 10^{12}$/l, and haemoglobin $10.7 \pm 0.27 \times$ g/dl decreased the MCV 71.34 ± 0.57 fl as compared to pure VC count of RBC $5.11 \pm 0.31 \times 10^{12}$/l, haemoglobin $7.36 \pm 0.29 \times$ g/dl, and MCV 89.53 ± 0.59 fl. The morphology of RBC in the pure VC and NFs group was spherical compared to the diseased group's microcytic shape. The neutropenia and lymphopenia were more prominent with VC administration and improved with the NFs group from 11.88 ± 1.29 to 24.78 ± 2.69% and 32.22 ± 2.89 to 45.48 ± 2.91%, respectively. WBC morphology of WBCs was abnormal in both VC groups; there was no significant difference in the platelet count of all groups of rats compared to the control group. The kidney function test showed that BUN was 24.66 ± 1.02 mg/dl and serum creatinine was 0.49 ± 0.20 mg/dl in the pure VC group as compared to NFs group

Table 5 Complete blood profile with hepatic and renal parameters in nanoformulations of VC-loaded TCs-HA compared to pure VC group ($n = 10$, mean + SD, $p \leq 0.05$)

Parameters	Control ($n = 10$)	Prostate cancer (n = 10)	Pure VC (n = 10)	VC-NFs (n = 10)	Range (Unit)
RBC profile					
RBC count	5.93 ± 0.27	3.41 ± 0.23	3.09 ± 0.29	5.11 ± 0.31	4–5.9 × 10^{12}/l
Haemoglobin	14.53 ± 0.25	9.22 ± 0.21	7.36 ± 0.29	10.7 ± 0.27	12–16 × g/dl
Haematocrit	46.67 ± 1.17	31.56 ± 1.15	31.34 ± 1.09	32.07 ± 1.19	35–50%
MCV	45.14 ± 0.59	100.12 ± 0.61	89.53 ± 0.59	71.34 ± 0.57	40–60 fl
MCH	24.67 ± 0.58	17.29 ± 0.59	16.48 ± 0.55	19.58 ± 0.56	21–31 pg
MCHC	31.33 ± 0.59	49.35 ± 0.55	46.24 ± 0.55	41.47 ± 0.56	30–39%
Haemolysis	2 ± 0	12.33 ± 0.4	25.83 ± 0.5	15.32 ± 0.3	0%
RBC morphology	Normal	Macrocytic	Spheroidal	Spheroidal	Normal
WBC Profile					
WBC count	7.37 ± 1.27	31.22 ± 1.25	1.01 ± 1.22	4.37 ± 1.17	4.5–11.0 × 10^3/µl
Neutrophils	4.21 ± 2.65	89.21 ± 2.48	11.88 ± 1.29	24.78 ± 2.69	21–57%
Lymphocytes	6.67 ± 3.06	92.67 ± 3.09	32.22 ± 2.89	45.48 ± 2.91	49–82%
Monocytes	1.67 ± 0.59	9.38 ± 0.55	0.99 ± 0.58	1.02 ± 0.51	1.7–4.3%
Eosinophils	2.33 ± 0.29	17.27 ± 0.27	10.22 ± 0.26	7.46 ± 0.26	0–3%
Basophils	2.33 ± 0.27	0.25 ± 0.26	0.57 ± 0.27	1.64 ± 0.27	0–3%
WBC morphology	Normal	Normal	Abnormal	Abnormal	Normal
Platelet profile					
Count	375,000 ± 0.39	480,000 ± 0.47	329,000 ± 0.43	367,000 ± 0.36	150,000–450,000 µl
Morphology	Normal	Normal	Normal	Normal	Normal
Kidney function test					
BUN	15.39 ± 0.19	28.29 ± 0.39	24.66 ± 1.02	18.45 ± 0.31	18–29 mg/dl
Creatinine	0.1 ± 0.01	0.37 ± 0.21	0.49 ± 0.20	0.38 ± 0.19	0.1–0.4 mg/dl
Liver function test					
ALT	14.32 ± 3.38	59.19 ± 3.68	48.39 ± 4.37	31.23 ± 4.85	4.1–36 U/L
AST	10.93 ± 2.27	35.25 ± 3.41	49.68 ± 2.44	25.66 ± 4.91	8.1–33 U/L
ALP	17.21 ± 2.46	48.26 ± 3.49	68.97 ± 2.57	36.33 ± 5.26	4.1–40 U/L

18.45 ± 0.31 mg/dlL and 0.38 ± 0.19 mg/dl, respectively, which showed comparatively less renal toxicity.

The ALT, AST, and ALP were 48.39 ± 4.37 U/l, 49.68 ± 2.44 U/l, and 68.97 ± 2.57 U/l in the pure VC group and showed severe vincristine-induced hepatotoxicity, but these parameters were improved 31.23 ± 4.85 U/l, 25.66 ± 4.91 U/l, and 36.33 ± 5.26 U/l, respectively, in NFs treatment animals as depicted in Table 5.

Antioxidant biomarkers

The serum samples were quantified for antioxidant enzyme levels in cancer and treatment groups compared to the control. The PC group's MDA level was 86.85 + 0.01 µmol/l while it decreased to 75.78 ± 0.02 to 61.93 ± 0.01 µmol/l in the pure VC and NFs of VC-loaded TCs-HA group. The GSH level was 0.28 ± 0.02 mmol/l in the diseased animal, while it was slightly reduced to 0.17 ± 0.01 and 0.19 ± 0.01 mmol/l in both groups, respectively. The PC animals showed 182.8 ± 0.01 U/ml SOD level, and treatment groups showed 160.6 ± 0.01 and 130.9 ± 0.02 U/ml in pure drug and respective NFs administered groups. The CAT level was 0.05 ± 0.01 U/ml in cancer and was slightly increased in the treatment group, as shown in Fig. 16.

Histopathological analysis

PC3 xenograft tumours and major organs, including lung, kidney, brain, liver, and heart from control and treated rats, were sectioned and stained with standard hematoxylin and eosin, as shown in Figs. 17 and 18. The tumour-bearing tissue showed large and irregular nuclei of malignant cells with scant cytoplasm and induction of angiogenesis in some areas with invasion to neighbouring stromal tissue. The brain showed significant signs of inflammation or toxicity, and liver and kidney cells showed some metastatic tumour foci and inflammation; however, the lung and heart showed minor signs of inflammation or toxicity in the pure VC-treated group of animals. After the NFs of VC-loaded TCs-HA treatment, a notable decline in necrosis and inflammation was observed in the liver, kidney, and brain. The VC-induced toxicity signs were seen in liver and kidney cells which were significantly lesser in NFs-treated rats than in the pure VC group. The tumour cells have a delicate, homogeneous nuclear chromatin pattern without prominent nucleoli or glandular formation.

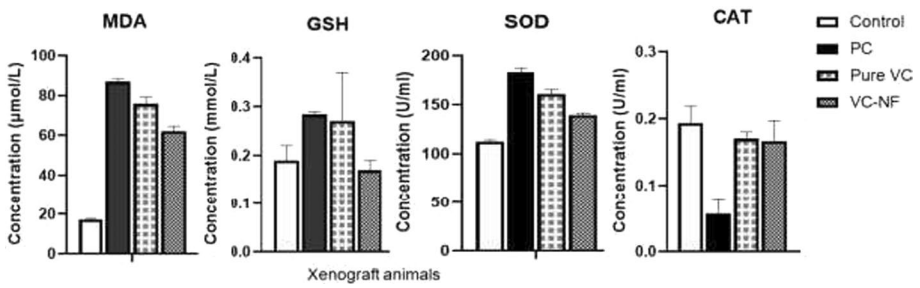

Fig. 16 Antioxidant enzyme (MDA, GSH, SOD, and CAT) levels were quantified at the end of the protocol in the PC group as compared to pure VC and NFs of VC-loaded TCs-HA treatment groups ($n = 10$, mean ± SD, $p \leq 0.05$)

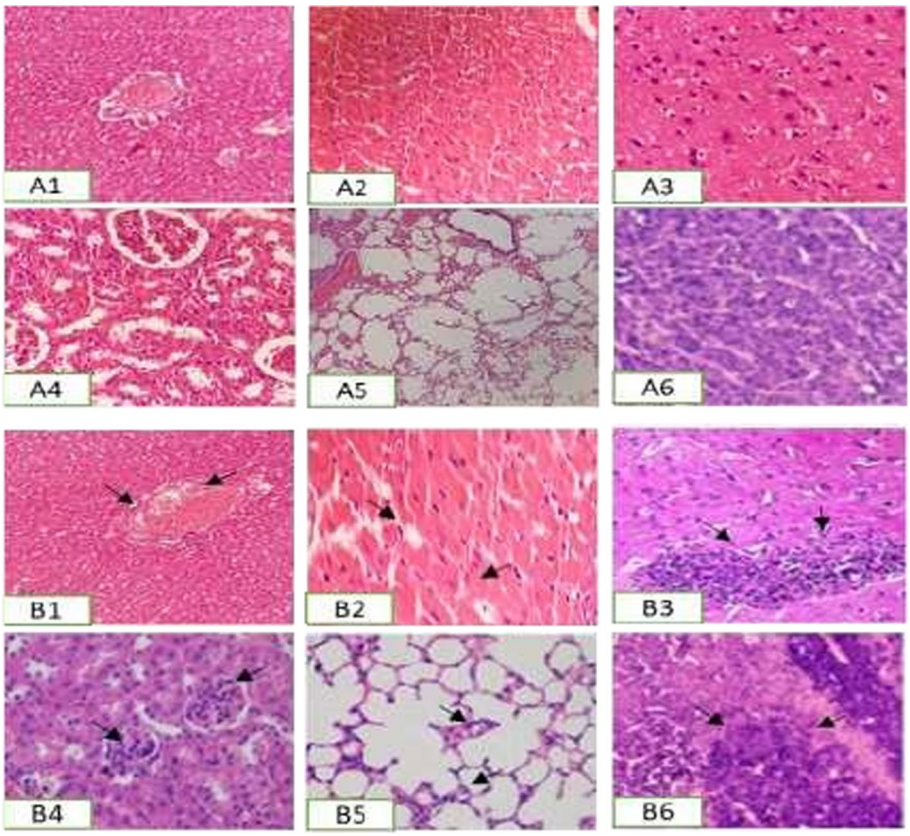

Fig. 17 Histopathology of the control group (liver: A1, heart: A2, brain: A3, kidney: A4, lung: A5, and before tumour area: A6), prostate cancer group (B1 to B6) showed very mild metastasis (non-significant) in the liver (B1) and kidney (B4), but tumour foci with blood vessel were significant in tumour side (B6)

Immunohistochemistry

Immunohistochemistry was conducted on xenografts tumours along with brain, heart, kidney, liver, and lung tissues from the control group, xenografts tumour group and treatment groups of pure VC and NFs group. The tissue samples were treated with COX-II, TNF-α, and NFκB antibodies to evaluate their expression in PC, treatment groups and control animals.

Image analysis showed the presence of malignant cells with high expressions of COX-II, TNF-α, and NFκB in their cytoplasm and nuclei on the 8th (B1) and 16th (B2) day in Figs. 20, 23 and 26, respectively). Brain sections, specifically the hippocampus, liver, and kidney, showed significant neuro, hepatic, and renal toxicities in the pure VC treatment group. NFs administered to rats revealed significantly lower neurotoxicity, hepatotoxicity, and renal toxicity and slightly reduced toxicities in the heart and lungs compared to VC treatment alone. COX-II and NFκB expression was lowered in cytoplasmic and nucleus concomitant with reduced inflammation, specifically in the brain, liver, and kidney. However, toxicity-induced inflammation in all organs showed slightly lesser protective effects of NFs on TNF-α expressions when compared to COX-II and NFκB expressions. Cytoplasmic staining of COX-II and TNF-α and nuclear staining of NFκB showed higher expressions in the PC group than in the control group. The expression of all three proteins

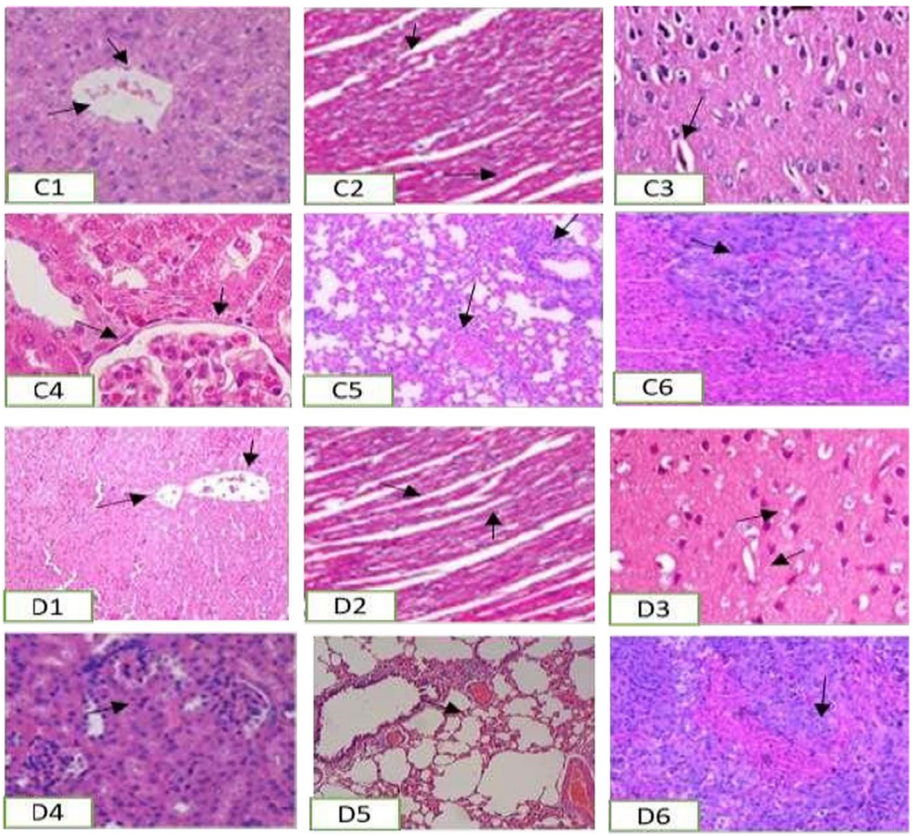

Fig. 18 Histopathology of the VC treatment group showed very significant neuro (C3), significant hepatic (C1) and renal (C4) and less significant cardio (C2) and lung toxicity(C5) compared to NFs of VC-loaded TCs-HA treatment group with lesser off-target toxicities (D1 to D5) and prominent cytotoxic effect at the tumour site with less angiogenesis and invasion (D6)

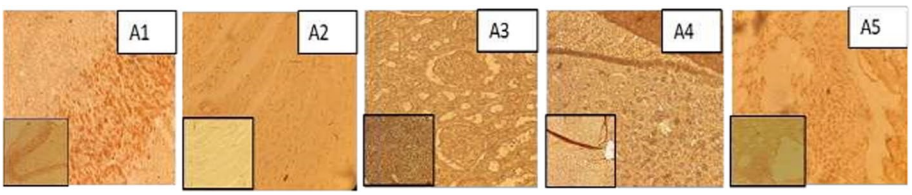

Fig. 19 COX-II immunohistochemistry results for control groups. Control group (brain: A1, heart: A2, kidney, A3, liver: A4, lung: A5) $n = 10$, mean + SD, $p \leq 0.05$. Images were taken at 10× and 40×

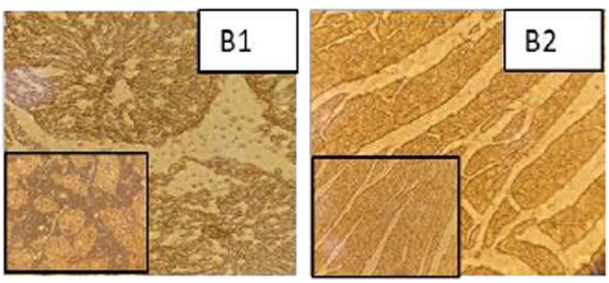

Fig. 20 The PC group showed metastasis on the 8th day (B1) and 16th day (B2) in the prostate cancer group via COX-II immunohistochemistry. $n = 10$, mean + SD, $p \leq 0.05$. Images were taken at 10× and 40×

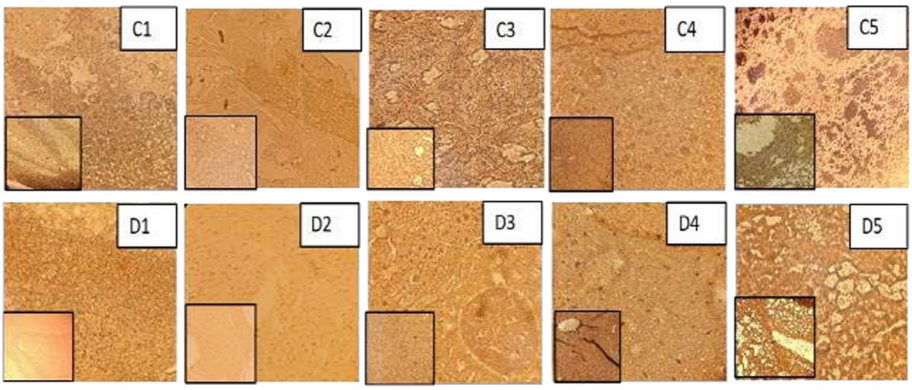

Fig. 21 Pure VC treatment groups showed severe toxicities, including significant neurotoxicity (C1), hepatotoxicity (C4) and renal toxicity (C3), with comparatively lesser toxicity seen in cardiac tissues (C2) and lung tissues (C5). However, VC-loaded TCs-HA NFs treatment groups showed reduced off-target toxicities (D1 to D5) with cytotoxic anti-tumour effects and a possibility of slower angiogenesis; $n = 10$, mean + SD, $p \leq 0.05$. Images were taken at 10 × and 40 ×

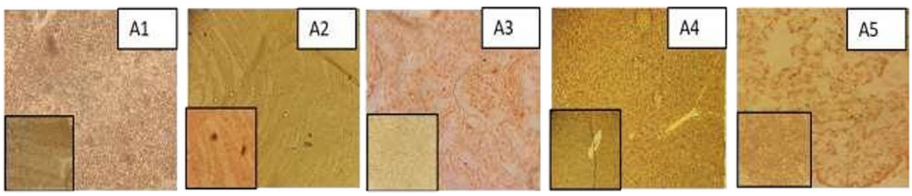

Fig. 22 TNF-α immunohistochemistry results for control groups. Control group (brain: A1, heart: A2, kidney, A3, liver: A4, lung: A5) n = 10, mean + SD, p ≤ 0.05. Images were taken at 10 × and 40 ×

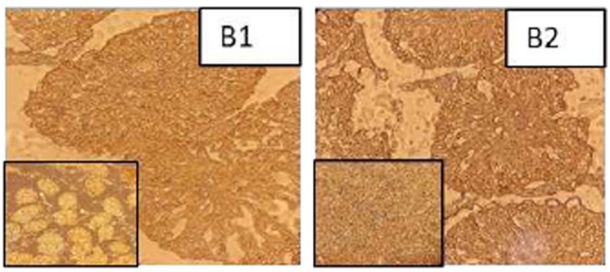

Fig. 23 The PC group showed metastasis on the 8th day (B1) and 16th day (B2) in the prostate cancer group via TNF-α immunohistochemistry. $n = 10$, mean + SD, $p \leq 0.05$. Images were taken at 10 × and 40 ×

decreased in the NFs group compared to the pure VC group (Figs. 19, 20, 21, 22, 23, 24, 25, 26, 27). Antibodies quantification was done by Image J, and images were taken at 10X and 40X (Fig. 28).

ELISA

The ELISA was performed to detect the protein expressions in the systemic circulation of xenograft rats, including Bax, BCL-2, cleaved PARP, and cleaved Caspase 3. The treatment of NFs and pure VC at 1 mg/kg induced the expression of Bax, cleaved Caspase 3, and cleaved PARP, while the expression of BCL-2 was significantly reduced, as shown in

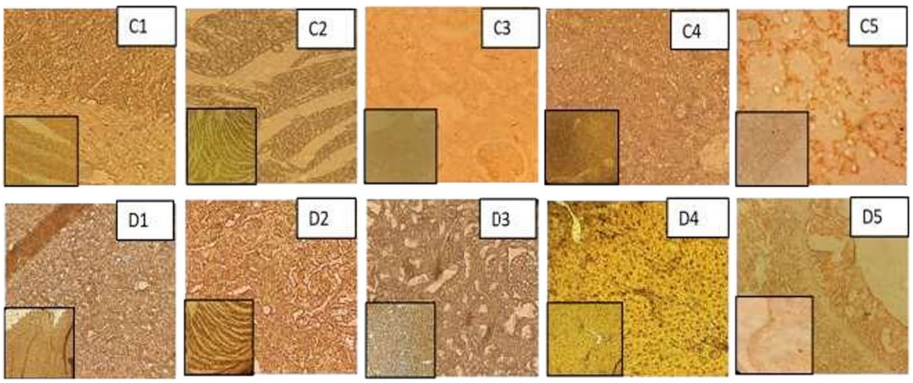

Fig. 24 Pure VC treatment groups showed severe toxicities, including significant neurotoxicity (C1), hepatotoxicity (C4) and renal toxicity (C3), with comparatively lesser toxicity seen in cardiac tissues (C2) and lung tissues (C5). However, VC-loaded TCs-HA NFs treatment groups showed reduced off-target toxicities (D1 to D5) with cytotoxic anti-tumour effects and a possibility of slower angiogenesis; $n = 10$, mean + SD, $p \leq 0.05$. Images were taken at 10 × and 40 ×

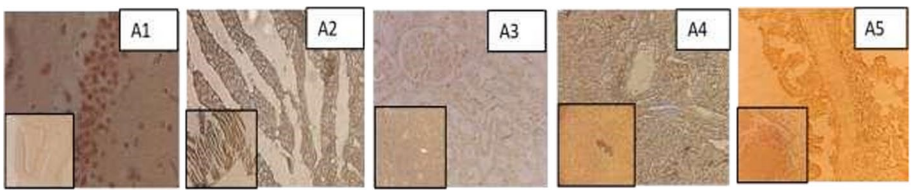

Fig. 25 NFκB immunohistochemistry results for control groups. Control group (brain: A1, heart: A2, kidney, A3, liver: A4, lung: A5) $n = 10$, mean + SD, $p \leq 0.05$. Images were taken at 10 × and 40 ×

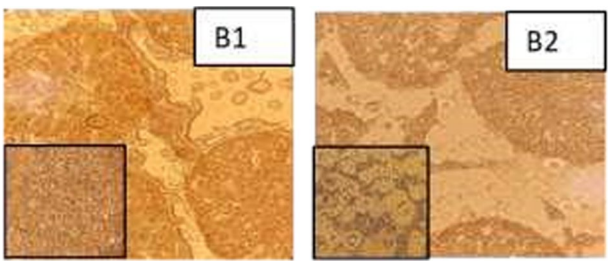

Fig. 26 The PC group showed metastasis on the 8th day (B1) and 16th day (B2) in the prostate cancer group via NFκB immunohistochemistry. $n = 10$, mean + SD, $p \leq 0.05$. Images were taken at 10 × and 40 ×

Fig. 29. These ELISA findings further support the more effective anticancer effect of NFs compared to pure VC.

The TNF-α protein expression was increased from 906 ± 0.07 to 3516.6 ± 0.19 pg/ml in the control to PC group and reduced expression in the NFs group compared to pure VC from 1425 ± 0.31 to 2208.3 ± 1.07 pg/ml. The expression of NFκB and COX-II was 0.37 ± 0.32 and 0.9 ± 0.11 in the control, 1.98 ± 0.25 and 2.06 ± 0.16 in the cancer group, 0.74 ± 1.14 and 1.45 ± 1.06 in pure VC and 0.48 ± 0.12 and 1.2 ± 0.08 in NFs group as shown in Fig. 30. All interactive protein expression was reduced in the NFs-treated group, leading to a more pronounced anticancer effect of NFs than pure VC in the tissues taken from xenograft cancer models.

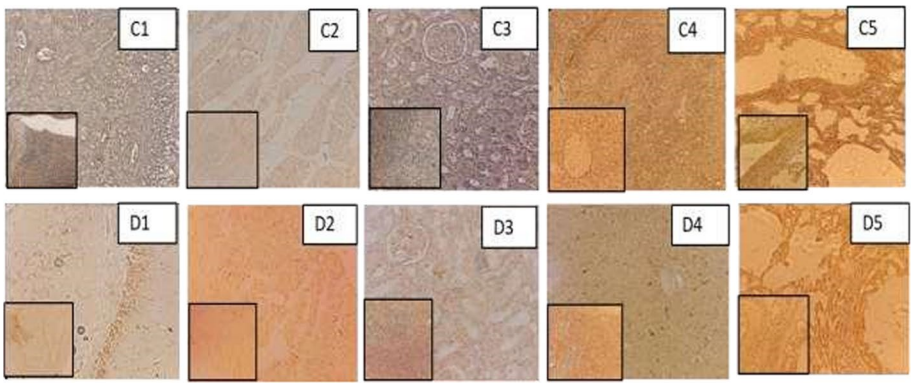

Fig. 27 Pure VC treatment groups showed severe toxicities, including significant neurotoxicity (C1), hepatotoxicity (C4) and renal toxicity (C3), with comparatively lesser toxicity seen in cardiac tissues (C2) and lung tissues (C5). However, VC-loaded TCs-HA NFs treatment groups showed reduced off-target toxicities (D1 to D5) with cytotoxic anti-tumour effects and a possibility of slower angiogenesis; $n = 10$, mean + SD, $p \leq 0.05$. Images were taken at 10 × and 40 ×

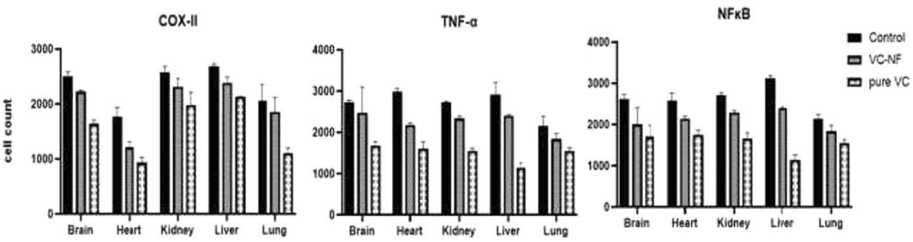

Fig. 28 Quantifying cell count with Image J after tissue treatment with primary antibodies COX-II, TNF-α and NFκB via immunohistochemistry protocols. $n = 10$, mean + SD, $p \leq 0.05$

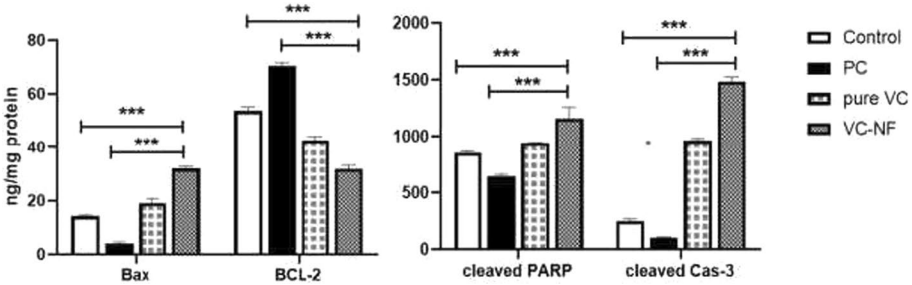

Fig. 29 Expression of Bax, BCL-2, cleaved PARP, and cleaved Caspase 3 was observed by ELISA in the PC group compared to pure VC and NFs of VC-loaded TCs-HA treatment groups ($n = 10$, mean ± SD, $p \leq 0.05$, *** highly significant)

Discussion

The current study explored in vitro and in vivo characterization of previously reported CD44 targeted vincristine-loaded thiolated chitosan NFs with an outer coating of hyaluronic acid (VC-loaded TCs-HA) (Naseer et al. 2022b). PC3-cell line and PC3-induced prostate cancer xenograft rat model were employed for this purpose. The purpose of selecting the PC3 among all other PC cell lines was its aggressive behaviour, a high expression for neuroendocrine (NE) markers, and stem cell-associated CD44 marker. In an in vitro cell morphology assay, apoptosis induced in PC3 treated with NFs of

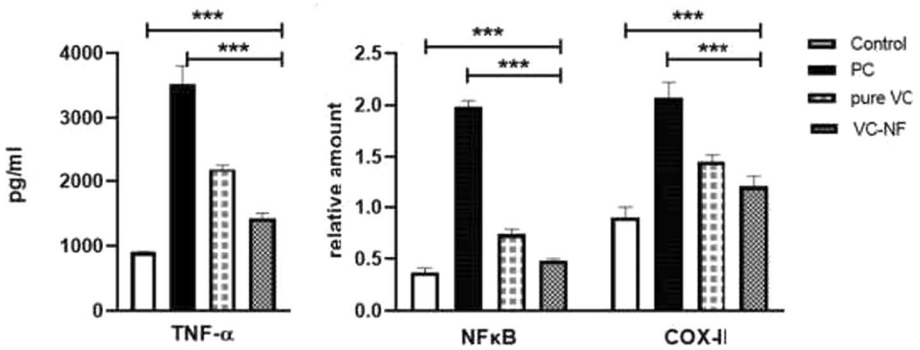

Fig. 30 Expression of specific proteins COX-II, NFκB, and TNF-α was quantified at the end of the protocol in the PC group compared to pure VC and NFs of VC-loaded TCs-HA treatment groups ($n = 10$, mean ± SD, $p \leq 0.05$, ***highly significant)

VC-loaded TCs-HA was comparable to cells treated with a drug alone, confirming that the new NFs produced could deliver the drug efficiently while the targeted delivery of the NFs spared the normal cells from the cytopathic effect of the drug. Cell viability was also reduced with increased concentration of the NFs and pure drug in normal and cancerous cell lines, as determined by the trypan blue exclusion assay. Similar in vitro results were reported using normal prostate HPrEC and cancerous cell line PC3 (Naseer et al. 2022b).

The simulated physicochemical and pharmacokinetic parameters VC using a cloud version of ADMET Predictor (TM) were studied at an initial dose of 1 mg/kg via the IV route. To check the authenticity of predicted values, the concentration of VC in rat plasma was measured by HPLC analysis after administration of NFs loaded with VC as compared to the pure drug. Significant differences in pharmacokinetic parameters and NFs displayed improved pharmacokinetic profiles. The HPLC analysis for the pharmacokinetic study of vincristine sulfate-loaded PLGA–PEG nanoparticle formulations after injection into rats showed similar improved kinetics and bioavailability in the earlier published study (Chen et al. 2011). The highly lipophilic compounds with logD >3.5 at 7.4 are likely to have poor aqueous solubility with high first-pass metabolism, leading to high in vivo clearance and low oral bioavailability. Lipinski said drug-like molecules should have log D values less than five for proper absorption and permeation (Lu et al. 2012). The cancer cells have a pKa of around 6.8, and the drug has maximum penetration in the cancer cells at this pKa value. Figure 4 also shows the relationship of VC at different pKa values; the most effective relationship was pKa 6.37, as the drug was 100% available. These are the representatives of the cancer cell environment and the typical physiological environment, as pKa values are direct correspondents of the pH values of the drug. These values showed the amount of drug available in the maximum amount at a particular pKa value. Drug metabolism studies are critical to uncovering new chemical entities by discovering active metabolites. A predictive metabolic profile is essential to limit predicted protection hazards due to the production of functional metabolic products that may be toxic, to ensure broad coverage of human metabolites in animals, to support dose prediction in humans, and to provide a preclinical metabolic profile in animals as compared to humans (Zhang and Tang 2018) (Table 6).

Table 6 Vincristine relationship with other metabolic enzymes

Parameter	Predicted value	Explanation
CYP2D6 inhibition	Yes (55%)	Predicts whether or not the compound is human CYP 2D6 inhibitor (Yes/No). Overall accuracy = 76%
CYP3A4 CLint	133.431 mg/min	Pooled atom-level intrinsic clearance in uL/min/mg HLM protein for CYP 3A4 mediated oxidation. RMSE/MAE = 0.67/0.53 log units
CYP3A4 human liver microsomes CLint	252.922 mg/min	Pooled atom-level intrinsic clearance in uL/min/mg HLM protein for CYP 3A4 mediated oxidation in human liver microsomes (unbound form). RMSE/MAE = 0.56/0.44 log units
CYP3A4 inhibition	Yes (80%)	Predicts whether or not the compound is human CYP 3A4 inhibitor (Yes/No). Overall accuracy = 78%
CYP3A4 Vmax	31.138 Moles/min	Kinetic Michaelis–Menten atom-level Vmax constants in nmol/min/(nmol of enzyme) for CYP 3A4 mediated oxidation. RMSE/MAE = 0.57/0.46 log units
CYP3A4 substrate	Yes (92%)	Predicts whether or not the compound is human CYP3A4 substrate (Yes/No). Overall accuracy = 82%
UGT1A3	Yes	Predicts whether or not the compound is substrate of UDP glucuronosyltransferase 1A3 (Yes/No). Overall accuracy = 86%

VC is a highly lipophilic drug with some polar groups, representing various ways to interact with transport proteins. The primary transport protein for VC across the cellular membranes was p glycoprotein, which means 99% of the drug's transport. Other proteins involved in the transport of VC across cellular membranes and tissues with different LogD values were OATP1B3 and OATP1B1, representing a significant association with VC's transport. The goal of toxicity testing is to identify any potential hazardous consequences that a drug entity may have, not merely to determine how safe it is, how drug compounds affect lab animals, and whether they have any direct hazardous effects on humans. They also include subjecting lab animals to high dosages to assess potential risks to humans exposed to much lower amounts (Arome and Chinedu 2013). The pharmacokinetic parameters are crucial for converting a drug molecule into a proper formulation that ultimately provides optimum efficacy with the least toxic effects. Several in silico tools are now used to determine pharmacokinetic parameters (Sui et al. 2008).

In the current study, potent immunosuppression was done by administering cyclosporine, ketoconazole, and cyclophosphamide. Jivrajani has used the same regimen for immunosuppression in C57BL/6 mice to induce tumours by subcutaneously injecting cells of human lung adenocarcinoma, prostate adenocarcinoma, and cervical adenocarcinoma and achieved a 100% success with no mortality (Jivrajani et al. 2014). Immunosuppression in rats was evident by a significant reduction in total WBC and lymphocyte count, and administration of cyclophosphamide suppressed the neutrophils. Ketoconazole and amoxicillin protected the immunosuppressed animals from bacterial and fungal infection, a significant cause of death in immunosuppression protocols. Compared to pure VC, the xenograft model was used to evaluate the targeted drug of VC-encapsulated NFs. There was a lesser increase in mean body weight, and mean tumour measurements were significantly decreased in NFs of VC-loaded TCs-HA compared to pure VC in xenograft rats. The polymeric micelles of paclitaxel were evaluated for safer high-dose drug therapy, and the in vivo anticancer activity showed the same pattern in the tumour growth achieved by subcutaneously injected A2780 cells in Balb/c rats (He et al. 2016).

The chemotherapeutic agents, including VC, cause microangiopathic haemolytic anaemia by mechanical destruction of red blood cells upon administration of high doses and long-term use (Michlitsch et al. 2019). Hence, the VC-loaded TCs-HA NFs have displayed two times lesser haemolysis in RBCs than pure VC at lesser concentrations. Therefore, NFs are less toxic to RBS and have a higher safety profile. The complete blood analysis showed an increase in the profiles of RBCs, WBCs, and platelets and a decrease in the liver and kidney function parameters with the administration of NFs of VC-loaded TCs-HA compared to pure VC in xenograft rats. In vivo xenograft, nude mice pharmacodynamics experiments showed that hyaluronic acid-paclitaxel increased the survival rate of mice, significantly reduced the density of microvessels in tumour tissues, and effectively inhibited the growth of tumours. At the same time, hyaluronic acid-PTX was more effective than paclitaxel-free drugs in treating intra-abdominal tumour density, eliminating ascites, and prolonging survival time in transplanted ovarian cancer cell lines (Lee et al. 2012). Some researchers made a new type of delivery system linking cisplatin and hyaluronic acid to increase the concentration of platinum in lymphatic vessels and reduce systemic toxicity and side effects while inhibiting early tumour metastasis. Compared with the free drug, hyaluronic acid cisplatin could increase the concentration of the drug in plasma and tissue to improve the distribution of the drug at the tumour site, significantly reducing renal toxicity (Liu et al. 2021).

The bioinformatics analysis showed the significant interaction of VC with some proteins, including Caspase-I, COX-II, NFκB, and TNF-α. Their high protein expression was confirmed by immunohistochemistry after staining with specific antibodies in the tissues of the disease group. Furthermore, a comparatively higher expression of these proteins was observed in the pure drug-treated group than in the NFs-treated group. ELISA further supplemented these results. To check the apoptotic pathways adopted by NFs of VC, the expression of Bax, BCL-2, cleaved PARP, and cleaved Caspase 3 was also observed and showed high levels of Bax and cleaved Caspase 3 and lower levels of BCL-2 and cleaved PARP in NFs-treated group which showed that VC-NFs retained its reported anticancer effect by cause proteolysis via caspase-dependent pathways. Subchronic administration of vincristine sulfate in rats induces nephrotoxicity via activation of Raf-1-MEK1/2-ERK1/2 signalling pathway leading to downregulation of Bcl2 and upregulation of P53, Bax, and cleaved Caspase-3 (Shati et al. 2019).

Some previous studies have shown that androgen-insensitive prostate cancer cells are also TNF-α insensitive but respond to NFκB via the activation of antiapoptotic genes. TNF-α has also been implicated in tissue remodelling and proliferation. This paradox is due to two separate and distinct TNF-α-mediated pathways in cells. One pathway leads to apoptosis, and the other to activating protective antiapoptotic genes through NFκB. Prostate cancer cells up-regulate multiple NFκB responsive genes in response to TNF-α stimulation (Han et al. 2021). These molecules may be involved in cell proliferation and metastasis, where modulation of their expression could be clinically beneficial. The results of this study strongly advocate that the off-target toxicities by VC in prostate tumours that otherwise showed pronounced organ toxicities would further be reduced by NFs of VC-loaded TCs-HA treatment revealing significantly lower inflammation, specifically in the brain, liver, and kidney along with slight protective effects in the lung and heart tissues as well.

Conclusions

This study supports that the novel NFs of VC-loaded TCs-HA are compelling for targeted and safer drug delivery for anticancer drugs. This novel formulation has improved pharmacokinetic, bioavailability and biodistribution profiles in healthy rats compared to pure VC, as determined by HPLC analysis of VC released at different time points and encapsulation efficacy. The targeted cytotoxic effect of NFs at lower doses was seen in cancer cells, along with reduced haemolytic and off-target toxicities in immunosuppressed xenograft rat models. For caspase-dependent apoptosis, these results were established by physiological, haematological, and antioxidant parameters evaluations, histopathology, immunohistochemistry, and ELISA-based confirmations. Simulated effects of VC molecular docking with Caspase-1, COX-II, NFκB, and TNF-α were confirmed by tissue analysis via immunohistochemical expressions of cellular inflammatory mediators (COXII, TNF-α, and NFκB). After that, it is concluded that the NFs of VC-loaded TCs-HA have a targeted effect on cancer cells and enhanced protective effects against VC-induced off-target toxicities, highlighting the attenuation of VC-related neurotoxicities, heptotoxicities, and nephrotoxicities in the prostate xenograft model.

Limitations

This study required further extensive molecular pathway detection following western blot and FACS analysis for specific antibodies expression observation and cell cycle-specific phase detection. These studies are in the pipeline for the completion of the project shortly.

Acknowledgements
We gratefully acknowledge the technical and financial support of the Deanship of Scientific Research (DSR) provided at King Abdulaziz University, Jeddah, Saudi Arabia under grant no. (FP-225-43).

Author contributions
FN: conceptualization, writing—original draft, writing and lab work. TA: supervision and proofreading. KK: in vitro analysis and writing. MSA: data analysis, methodology and funding. SA: supervision and proofreading.

Availability of data and materials
Data will be made available on request.

Declarations

Ethics approval and consent to participate
Ethical approval/IRB letter no. 04-2022-ASAB-01/02 from the National University of Sciences and Technology Islamabad (NUST), Islamabad, Pakistan, attached here for reference**.**

Consent for publication
All authors agreed to the publication of the manuscript.

Competing interests
The authors declare no conflict of interest in this study.

Received: 3 December 2022 Accepted: 2 June 2023
Published: 20 June 2023

References:

Aghasizadeh M, Moghaddam T, Bahrami A, Sadeghian H, Alavi S, Matin M (2022) 8- Geranyloxycarbostyril as a potent 15-LOX-1 inhibitor showed great anti-tumor effects against prostate cancer. Life Sci 293:120272
Ahlmann M, Hempel G (2016) The effect of cyclophosphamide on the immune system: implications for clinical cancer therapy. Cancer Chemother Pharmacol 78(4):661–671
Amar S, Eryilmaz R, Demir H, Aykan S, Demir C (2019) Determination of oxidative stress levels and some antioxidant enzyme activities in prostate cancer. Aging Male 22(3):198–206
Arome D, Chinedu E (2013) The importance of toxicity testing. J Pharm BioSci 4:146–148

Chen J, He H, Li S, Shen Q (2011) An HPLC method for the pharmacokinetic study of vincristine sulfate loaded PLGA-PEG nanoparticle formulations after injection to rats. J Chromatogr B Analyt Technol Biomed Life Sci 879(21):1967–1972
Davis AM, Riley RJ (2004) Predictive ADMET studies, the challenges and the opportunities. Curr Opin Chem Biol 8(4):378–386
Firestone B (2010) The challenge of selecting the 'right' in vivo oncology pharmacology model. Curr Opin Pharmacol 10:391–396
Ghaferi M, Amari S, Mohrir BV, Raza A, Shahmabadi HE, Alavi SE (2020) Preparation, Characterization, and Evaluation of Cisplatin-Loaded Polybutylcyanoacrylate Nanoparticles with Improved In Vitro and In Vivo Anticancer Activities. Pharmaceuticals (Basel) 13(3):44
Han JH, Park J, Kang TB, Lee KH (2021) Regulation of caspase-8 activity at the crossroads of pro-inflammation and anti-inflammation. Int J Mol Sci 22(7):3318
He Z, Wan X, Schulz A, Bludau H, Dobrovolskaia M, Stern S, Montgomery S, Yuan H (2016) A high capacity polymeric micelle of paclitaxel: implication of high dose drug therapy to safety and in vivo anticancer activity. Biomaterials 101:296–309
Iyengar A, Kamath N, Phadke KD, Bitzan M (2013) Cyclosporine/ketoconazole reduces treatment costs for nephrotic syndrome. Indian J Nephrol 23:419–423
Jahan F, Zaman S, Arshad R, Tabish A, Naseem AA, Shahnaz G (2021) Mapping the potential of thiolated pluronic based nanomicelles for the safe and targeted delivery of vancomycin against staphylococcal blepharitis. J Drug Deliv Sci Technol 61:102220
Jalilian M, Derakhshandeh K, Kurd M, Lashani H (2021) Targeting Solid Lipid Nanoparticles with Anisamide for Docetaxel Delivery to Prostate Cancer: Preparation, Optimization, and In-vitro Evaluation. Iran J Pharm Res 20(1):327–338
Jeswani G, Paul S, Ajazuddin B, Deshmukh R (2021) Design of vincristine sulfate loaded poloxamer in situ nanogel: formulation and in vitro evaluation. J Drug Deliv Sci Technol 61:102246
Jivrajani M, Shaikh MV, Shrivastava N, Nivsarkar M (2014) An improved and versatile immunosuppression protocol for the development of tumor xenograft in mice. Anticancer Res 34:7177–7184
Kousar K, Naseer F, Abduh MS, Anjum S and Ahmad T (2023) CD44 targeted delivery of oncolytic Newcastle disease virus encapsulated in thiolated chitosan for sustained release in cervical cancer: a targeted immunotherapy approach. Front Immunol 14:1175535. https://doi.org/10.3389/fimmu.2023.1175535
Kousar K, Naseer F, Abduh MS, Kakar S, Gul R, Anjum S, Ahmad T (2023) Green synthesis of hyaluronic acid coated, thiolated chitosan nanoparticles for CD44 targeted delivery and sustained release of Cisplatin in cervical carcinoma. Front Pharmacol 13:1073004. https://doi.org/10.3389/fphar.2022.1073004
Lee DE, Kim AY, Hong YY, et al. (2012) Amphiphilic hyaluronic acid-based nanoparticles for tumor-specific optical/MR dual imaging. J Mater Chem 22:10444–10447
Liu C, Wong S, Tai C, Tai C, Pan Y, Hsu H, Richardson C, Lin L (2021) Ursolic Acid and Its Nanoparticles Are Potentiators of Oncolytic Measles Virotherapy against Breast Cancer Cells. Cancers (Basel) 13(1):136
Lu D, Chambers P, Wipf P, Xie XQ, Englert D, Weber S (2012) Lipophilicity screening of novel drug-like compounds and comparison to clog P. J Chromatogr A 5(1258):161–167
McLean DT, Strand DW, Ricke WA (2017) Prostate cancer xenografts and hormone induced prostate carcinogenesis. Differentiation 97:23–32
Meanwell NA (2011) Improving drug candidates by design: a focus on physicochemical properties as a means of improving compound disposition and safety. Chem Res Toxicol 24(9):1420–1456
Michlitsch J, Larkin S, Vichinsky E, Kuypers FA (2019) Vincristine-induced anemia in hereditary spherocytosis. Exp Biol Med 244(10):850–854. https://doi.org/10.1177/1535370219853791
Naseer F, Ahmad T, Kousar K, Anjum S (2021) Advanced therapeutic options for treatment of metastatic castration-resistant prostatic adenocarcinoma front. Pharmacology 12:728054
Naseer F, Ahmad T, Gul R, Anjum S (2022a) Serendipity for the intervention of COVID-19 and prostatic adenocarcinoma (PC) pros. Canc Prostatic Dis 10:1–3
Naseer F, Ahmad T, Kousar K, Kakar S, Gul R, Anjum S, Shareef U (2022b) Formulation of surface-functionalized hyaluronic acid-coated thiolated chitosan nanoformulation for the delivery of vincristine in prostate cancer: a multifunctional targeted drug delivery approach. J Dru Del Sci Technol 74:1035–1045
Naseer F, Ahmad T, Kousar K, Kakar S, Gul R, Anjum S, Shareef U (2022c) Formulation for the targeted delivery of a vaccine strain of oncolytic measles virus (OMV) in hyaluronic acid coated thiolated chitosan as a green nanoformulation for the treatment of prostate cancer: a Viroimmunotherapeutic approach. Int J Nanomed. https://doi.org/10.2147/IJN.S386560
Naseer F, Ahmed M, Majid A, Kamal W, Phulle A (2022d) Green nanoparticles as multifunctional nanomedicines: insights into anti-inflammatory effects, growth signalling and apoptosis mechanism in cancer. Sem Can Biol 3:115
Shahzadi T, Zaib M, Riaz T, Shehzadi S, Abbasi MA, Shahid M (2019) Synthesis of eco-friendly cobalt nanoparticles using *Celosia argentea* plant extract and their efficacy studies as antioxidant, antibacterial, hemolytic and catalytical agent. Arab J Sci Eng. https://doi.org/10.1007/s13369-019-03937-0
Shao J, Wang C, Li L, Liang H, Dai J, Ling X, Tang H (2018) Luteoloside inhibits proliferation and promotes intrinsic and extrinsic pathway-mediated apoptosis involving MAPK and mTOR signaling pathways in human cervical cancer cells. Int J Mol Sci 19(6):1664
Shati A (2019) Sub-chronic administration of vincristine sulfate induces renal damage and apoptosis in rats via induction of oxidative stress and activation of Raf1-MEK1/2- Erk1/2 signal transduction. Int J Morphol 37(1):273–283
Silverman JA, Deitcher SR (2013) Marqibo® (vincristine sulfate liposome injection) improves the pharmacokinetics and pharmacodynamics of vincristine. Cancer Chemother Pharmacol 71:555–564
Silvestro I, Francolini I, Lisio VD, Martinelli A, Pietrelli L, et al (2020) Preparation and characterization of TPP-chitosan crosslinked scaffolds for tissue engineering. Materials 13:3577.
Škubník J, Jurášek M, Ruml T, Rimpelová S (2020) Mitotic poisons in research and medicine. Molecules 25:4632
Sui X, Sun J, Wu X, Li H, Liu J, He Z (2008) Predicting the volume of distribution of drugs in humans. Curr Drug Metab 9(6):574–580

Taymouri S, Varshosaz J, Javanmard SH, Hassanzadeh F (2018) Development of a rapid and precise reversed-phase high-performance liquid chromatography method for analysis of docetaxel in rat plasma: application in single-dose pharmacokinetic studies of folate-targeted micelles containing docetaxel. Adv Biomed Res 7:76–95
Trott O, Olson AJ (2010) AutoDock Vina: improving the speed and accuracy of docking with a new scoring function, efficient optimization, and multithreading. J Comput Chem 31(2):455–461
Verma A, Verma M, Singh A (2020) Animal tissue culture principles and applications. In: Verma AS, Singh A (eds) Animal biotechnology. Academic Press, Cambridge, pp 269–293
Yu H, Tang Z, Zhang D, Song W, Zhang Y, Yang Y, Ahmad Z, Chen X (2015) Pharmacokinetics, biodistribution and in vivo efficacy of cisplatin loaded poly(L-glutamic acid)-g-methoxy poly(ethylene glycol) complex nanoparticles for tumor therapy. J Control Release 10(205):89–97
Zhang Z, Tang W (2018) Drug metabolism in drug discovery and development. Acta Pharmaceutica Sinica b 8(5):721–732

Publisher's Note